HHS Public Access

Author manuscript

Immunity. Author manuscript; available in PMC 2021 April 14.

Published in final edited form as:

Immunity. 2020 April 14; 52(4): 606–619.e6. doi:10.1016/j.immuni.2020.02.009.

Interleukin-33 induces the enzyme tryptophan hydroxylase 1 to promote inflammatory group 2 innate lymphoid cell-mediated immunity

Anne-Laure Flamar[1,8], **Christoph S.N. Klose**[1,2,8], **Jesper B. Moeller**[1,3], **Tanel Mahlakõiv**[1], **Nicholas J. Bessman**[1], **Wen Zhang**[1], **Saya Moriyama**[1], **Vladislava Stokic-Trtica**[2,4], **Lucille C. Rankin**[1], **Gregory Garbès Putzel**[1], **Hans-Reimer Rodewald**[5], **Zhengxiang He**[6], **Lili Chen**[6], **Sergio A. Lira**[6], **Gerard Karsenty**[7], **David Artis**[1,9,10,*]

[1]Jill Roberts Institute for Research in Inflammatory Bowel Disease, Joan and Sanford I. Weill Department of Medicine, Department of Microbiology and Immunology, Weill Cornell Medicine, Cornell University, New York, NY 10021, USA

[2]Department of Microbiology, Infectious Diseases and Immunology, Charité - Universitätsmedizin Berlin, 12203 Berlin, Germany

[3]Department of Molecular Medicine, University of Southern Denmark, 5000 Odense, Denmark

[4]Max-Planck Institute for Infection Biology, Berlin, Germany

[5]Division of Cellular Immunology, German Cancer Research Center, 69120 Heidelberg, Germany.

[6]Precision Immunology Institute, Icahn School of Medicine at Mount Sinai, New York, NY 10029, USA

[7]Department of Genetics and Development, Columbia University Irving Medical Center, New York, NY 10032, USA

[8]These authors contributed equally

[9]Senior author

[10]Lead contact

Summary

[*]**Correspondence:** David Artis, Ph.D., Weill Cornell Medicine, Cornell University, Joan and Sanford I. Weill Department of Medicine, Belfer Research Building, Room 724 (box 210), 413 East 69th Street, New York, NY 10021, USA, Tel: 1-646-962-6291, dartis@med.cornell.edu.

Authorship contributions

A.-L.F. and C.S.N.K. carried out most experiments and analyzed the data with the help of J.B.M., T.M, N.J.B., W.Z., V.S.-T. , L.C.R. and S.M. G.G.P. performed RNA-seq analysis. H.-R.R., L.C., Z.H., S.A.L. and G.K. provided crucial mice for the study. A.-L.F., C.S.N.K. and D.A conceived the project and wrote the manuscript with input from all co-authors. D.A. directed and financed the research.

Declaration of interests

Although not related to this study, in the last twelve months D.A. has contributed to scientific advisory boards at Genentech, Pfizer, Takeda, FARE, and the KRF. All other authors declare no competing interests.

Group 2 innate lymphoid cells (ILC2s) regulate immunity, inflammation and tissue homeostasis. Two distinct subsets of ILC2s have been described: steady-state natural ILC2s and inflammatory ILC2s, which are elicited following helminth infection. However, how tissue-specific cues regulate these two subsets of ILC2s and their effector functions remains elusive. Here, we report that interleukin-33 (IL-33) promotes the generation of inflammatory ILC2s ($ILC2^{INFLAM}$) via induction of the enzyme tryptophan hydroxylase 1 (Tph1). Tph1 expression was up-regulated in ILC2s upon activation with IL-33 or following helminth infection in an IL-33-dependent manner. Conditional deletion of *Tph1* in lymphocytes resulted in selective impairment of $ILC2^{INFLAM}$ responses and increased susceptibility to helminth infection. Further, RNA sequencing analysis revealed altered gene expression in Tph1 deficient ILC2s including inducible T-cell co-stimulator (*Icos*). Collectively, these data reveal a previously unrecognized function for IL-33, Tph1 and ICOS in promoting inflammatory ILC2 responses and type 2 immunity at mucosal barriers.

eTOC blurb:

IL-33 is a potent activator of type 2 immune responses via the stimulation of ILC2s, but the downstream pathways triggered in these cells are poorly defined. Flamar and colleagues show that IL-33 controls tryptophan hydroxylase 1 expression in ILC2s, which is required for type 2 immunity against worm infections.

Introduction

Immunity at body's barrier surfaces is mediated by a wide array of tissue-resident immune cells, which constitute a first line of defense against infection (Fan and Rudensky, 2016; Klose and Artis, 2016; Rankin and Artis, 2018). Innate lymphoid cells (ILCs) are primarily tissue-resident lymphocytes, which are enriched at barrier surfaces (Gasteiger et al., 2015; Moro et al., 2016; Peng et al., 2013), and have emerged as important regulators of immunity, inflammation and tissue homeostasis (Artis and Spits, 2015; Eberl et al., 2015; Klose and Artis, 2016; Vivier et al., 2018). ILCs share functional diversity with helper T cells, characterized by the expression of similar lineage-specifying transcription factors and effector molecules. Although ILCs lack antigen-specific receptors, their localization at barrier surfaces allows them to quickly react to pathogenic and environmental stimuli (Diefenbach et al., 2014; Klose and Artis, 2016; Spits et al., 2013; Vivier et al., 2018).

Group 2 ILCs (ILC2s) have high expression of the lineage-specifying transcription factor GATA-3 and mediate diverse functions by producing a wide variety of cytokines and growth factors, such as interleukin (IL)-4, IL-5, IL-9, IL-13, amphiregulin. However, it is unknown whether individual populations of ILC2s produce all these effector molecules or whether functionally distinct ILC2 subsets are present in tissues. Similar to T helper-2 (Th2) cells, ILC2s trigger type 2 inflammation and have been implicated in many physiological and pathophysiological processes, including resistance to helminth infections, allergic inflammation, metabolic homeostasis, fibrosis and tissue repair (Hoyler et al., 2012; Klose and Artis, 2016; McHedlidze et al., 2013; Mjosberg et al., 2012; Monticelli et al., 2015; Monticelli et al., 2011; Moro et al., 2010; Neill et al., 2010; Spits et al., 2013; Vivier et al., 2018). ILC2s are activated via engagement of stimulatory receptors including glucocorticoid-induced tumor necrosis factor receptor (GITR) and inducible T-cell co-

stimulator (ICOS) (Maazi et al., 2015; Nagashima et al., 2018; Paclik et al., 2015) and by cytokines, such as IL-25, IL-33 and thymic stromal lymphopoietin (Artis and Spits, 2015; Eberl et al., 2015; Klose and Artis, 2016; Vivier et al., 2018). Recently, it has been reported that in the context of infection with the nematode *Nippostrongylus brasiliensis* (*N.brasiliensis*) or after injection of recombinant IL-25 (rIL-25), a second population of ILC2s is induced in the lungs and mesenteric lymph nodes (mesLN), termed inflammatory ILC2s ($ILC2^{INFLAM}$) as opposed to natural ILC2 ($ILC2^{NAT}$), which reside in these tissues at steady state (Huang et al., 2015). Phenotypically, $ILC2^{INFLAM}$ have high expression of the activation marker KLRG1 and IL-25 receptor (IL-17RB), but low expression of IL-33 receptor ST2 (T1) (Huang et al., 2015). Notably, $ILC2^{INFLAM}$ are thought to differentiate from intestinal ILC2s (Huang et al., 2015; Huang et al., 2018). However, how $ILC2^{INFLAM}$ subset is generated remains poorly understood.

IL-33 is an alarmin secreted by various cell types upon cell damage and is an important mediator of homeostasis of ILC2s and other immune cells in many tissues including, but not limited to, the intestine, lung, adipose tissue and skin (Brestoff et al., 2015; Halim et al., 2012; Kim et al., 2013; Mahlakoiv et al., 2019; Molofsky et al., 2015a; Monticelli et al., 2011; Moro et al., 2010; Rak et al., 2016). IL-33 plays a pivotal role in anti-helminth immunity (Hung et al., 2013; Moro et al., 2010; Price et al., 2010). Further, IL-33 is closely linked to detrimental immune responses, such as allergic inflammation in mice and human (Halim et al., 2014; Imai et al., 2013; Li et al., 2015; Moffatt et al., 2010; Molofsky et al., 2015b; Salimi et al., 2013). Therefore, IL-33 and its receptor, ST2, expressed on ILC2s are central in the regulation of type 2 inflammation in health and disease.

Although transcriptome of mouse and human ILC2s in different tissues have been studied (Bjorklund et al., 2016; Gury-BenAri et al., 2016; Ricardo-Gonzalez et al., 2018; Robinette et al., 2015; Simoni et al., 2017; Yudanin et al., 2019), how population heterogeneity of ILC2s impacts the outcome of protective or pathologic immune responses remains elusive. Our work identified IL-33 as an important regulator of ILC2 subset heterogeneity in the mucosa, and in particular, for the transition to $ILC2^{INFLAM}$ upon helminth infection. Furthermore, stimulation of ILC2s by IL-33 treatment or following *N. brasiliensis* infection resulted in the up-regulation of the transcript for tryptophan hydroxylase 1 (*Tph1*), the rate limiting enzyme in serotonin biosynthesis. Likewise, up-regulation of *Tph1* was dependent on IL-33. Moreover, conditional deletion of *Tph1* in lymphocytes resulted in defective $ILC2^{INFLAM}$ responses and impaired expulsion of *N. brasiliensis*. Mechanistically, *Tph1*-deficiency was associated with delayed recruitment of $ILC2^{INFLAM}$ to the mesenteric lymph nodes and altered expression of genes associated with co-stimulation and immune activation, including *Icos*, which was required for the generation of $ILC2^{INFLAM}$. Altogether, our data provide evidence of a previously unrecognized IL-33-Tph1-$ILC2^{INFLAM}$ pathway regulating type 2 immunity.

Results

IL-33 regulates inflammatory ILC2s

To study how IL-33 regulates tissue heterogeneity of the ILC2 subsets during type 2 inflammation, we infected IL-33-deficient ($Il33^{-/-}$) and $Il33^{+/+}$ mice with the intestinal

worm parasite *N. brasiliensis* and performed flow cytometry analysis of ILC2s from the mesLN using the published markers KLRG1 and CD25 (IL-2Rα chain) to identify ILC2s (Hoyler et al., 2012). Of note, in addition to lineage negative (Lin^-) $KLRG1^+$ $CD25^+$ $ST2^+$ ILC2 subset (termed natural ILC2s, $ILC2^{NAT}$) present in naïve mice, *N. brasiliensis* infection elicited a second population of Lin^- $KLRG1^+$ cells, which were $CD25^-$ and $ST2^-$ (termed inflammatory ILC2s, $ILC2^{INFLAM}$), and which were reduced in *Il33*$^{-/-}$ mice on day 7 and day 10 following infection with *N. brasiliensis* (Fig. 1a–f; Suppl. Fig. 1a–d). In addition, intestinal worm burden was significantly higher on day 7 and day 10 post-infection in *Il33*$^{-/-}$ mice as previously published (Hung et al., 2013), suggesting that the IL-33-dependent generation of $ILC2^{INFLAM}$ could be important for worm expulsion (Fig. 1c,f). Phenotypically, $KLRG1^+$ $CD25^-$ cells were $CD127^{low}$ $CD90^{low}$ Sca-1^{low} c-Kit^+ $ST2^-$ $CCR9^{high}$, consistent with previous reports in the literature (Fig. 1g) (Huang et al., 2015; Huang et al., 2018).

Next, we tested whether administration of recombinant IL-33 (rIL-33) could promote $ILC2^{INFLAM}$ generation. Four days after administration of rIL-33, we detected increased frequencies of $KLRG1^+$ $CD25^-$ $ILC2^{INFLAM}$ in the mesLN of wild-type mice, which were barely detectable in PBS-treated mice (Fig. 1h,i and Suppl. Fig. 1e–h). Since $ILC2^{INFLAM}$ were initially reported to be elicited upon IL-25 administration (Huang et al., 2015), we compared the capacity of IL-25 and IL-33 at stimulating $ILC2^{INFLAM}$ *in vivo*. While both cytokines were capable of eliciting $ILC2^{INFLAM}$, rIL-25 treatment resulted in a stronger recruitment of $ILC2^{INFLAM}$ to mesLN (Suppl. Fig. 1i,j). Moreover, injection of rIL-33 in IL-25 receptor-deficient (*Il17rb*$^{-/-}$) mice resulted in diminished induction of $ILC2^{INFLAM}$ compared to wild-type mice, suggesting that the two cytokines might cooperatively elicit $ILC2^{INFLAM}$ responses (Suppl. Fig. 1k,l). To further dissect how IL-25 and IL-33 support the generation of $ILC2^{INFLAM}$, we carried out *in vitro* cultures using sort-purified ILC2s from small intestinal (Si) lamina propria and tested whether combinations of the two cytokines promote down-regulation of ST2, a hallmark of $ILC2^{INFLAM}$. Addition of recombinant IL-33 to the culture medium resulted in modest down-regulation of ST2, whereas stimulation with IL-25 lead to strong up-regulation of ST2 (Fig. 1j,k). In contrast, *in vitro* cultures of ILC2s together with rIL-33 and rIL-25 resulted in a loss of ST2 expression comparable to that of ST2-deficient (*Il1rl1*$^{-/-}$) ILC2s (Fig. 1j). Therefore, taken together these data strongly suggest that IL-25 and IL-33 are both required and jointly promote $ILC2^{INFLAM}$ induction.

Since $ILC2^{INFLAM}$ are thought to originate from ILC2 in the intestine (Huang et al., 2015; Huang et al., 2018), we analyzed transgenic mice, which over-express IL-33 selectively under the villin promoter in intestinal epithelial cells (*Vfl33*) (He et al., 2018). Consistent with our previous findings, more $ILC2^{INFLAM}$ were recovered from the mesLN of *Vfl33* mice compared to wild-type control mice suggesting that tissue-specific expression of IL-33 in the intestine is sufficient to promote generation of $ILC2^{INFLAM}$ (Fig. 1l,m).

To investigate the heterogeneity of $ST2^-$ ILC2s in tissues, we purified leukocytes from the lung, epididymal white adipose tissue (eWAT), mesLN, Si and colon lamina propria of wild-type mice, and analyzed ST2 expression on ILC2s among these different tissues. $KLRG1^+$ ILC2s were predominantly $ST2^+$ at steady state in all tissues examined, except in the Si, in

which a significant proportion of ILC2s were ST2^{-} (Suppl. Fig. 1m,n). We hypothesized that the down-modulation of ST2 might already occur at steady state in the Si in response to the IL-33 receptor being constantly engaged by IL-33. Indeed, immunofluorescence staining revealed that IL-33 was constitutively highly expressed in Si mucosa (Suppl. Fig. 1o). We next investigated whether IL-33 affects ST2 expression in Si lamina propria at steady state using *Il33*$^{-/-}$ mice. As expected, a higher proportion of Si ILC2s expressed ST2 in *Il33*$^{-/-}$ mice compared to *Il33*$^{+/+}$ mice, suggesting that ILC2s are constantly activated by IL-33, resulting in down-modulation of ST2 expression on ILC2s even at steady state in the intestine (Fig. 1n,o). Similar analysis in *Il17rb*$^{-/-}$ mice revealed reduced frequencies of ST2^{-} ILC2s in the Si lamina propria compared to wild-type control mice (Fig. 1p,q). Collectively, we conclude from these experiments that IL-33 and IL-25 cooperatively induce the generation and are required for the induction of ILC2^{INFLAM} following *N. brasiliensis* infection.

Tph1 is expressed in ILC2s and up-regulated upon cell activation

To identify genes closely linked to ILC2 activation, we treated wild-type mice with PBS or rIL-33 and compared the transcriptome of sort-purified Si ILC2s. As expected, activation of Si ILC2s resulted in the up-regulation of genes associated with proliferation (*Mki67*) and effector cytokines (*Il5, Il13* and *Areg*) (Fig. 2a). One of the genes that exhibited most striking differential expression between control and rIL-33-treated animals was the transcript for tryptophan hydroxylase 1 (*Tph1*), the rate-limiting enzyme in serotonin biosynthesis (Fig. 2a, b). Up-regulation of *Tph1* mRNA expression after rIL-33 treatment was confirmed by quantitative PCR (qPCR) and flow cytometry analyses, and was specific to Si ILC2s since we did not detect expression of *Tph1* in other immune cells including Th2 cells, regulatory T (Treg) cells and mononuclear phagocytes (Fig. 2c–f). We verified that Si ILC2s were able to produce serotonin (5-hydroxytryptamine, 5-HT) *in vitro* as measured by ELISA from culture supernatants and *ex vivo* by immunofluorescence (Suppl. Fig. 2a,b). Expression of *Tph1* in Si ILC2s was independent of intestinal microbiota since germ-free (GF) mice had comparable *Tph1* mRNA expression as mice kept under specific-pathogen-free (SPF) conditions (Fig. 2g). Besides being highly up-regulated after ILC2 activation, the gene *Tph1* drew our attention because it was selectively expressed in ILC2s at steady state, but not in other innate and adaptive lymphocytes we examined (Fig. 2h,i), consistent with previous data reporting that *Tph1* is regulated by the lineage-specifying transcription factor for ILC2s, GATA-3 (Robinette et al., 2015; Yagi et al., 2014). In addition, *Tph1* mRNA expression in ILC2s was comparable to that of mast cells (Nowak et al., 2012; Ringvall et al., 2008) and higher in enterochromaffin cells, which express chromogranin A (*Chga*) and represent the main source of serotonin in the gastrointestinal tract (Gershon, 2013; Lund et al., 2018; Yadav et al., 2008) (Fig. 2j and Suppl. Fig. 2c). Small intestinal ILC2s had the highest *Tph1* mRNA expression compared to ILC2s derived from other tissues at steady state (Fig. 2k). Furthermore, *Tph1* mRNA expression was significantly higher in ILC2^{NAT} compared to ILC2^{INFLAM}, suggesting that *Tph1* mediates the transition of ST2^{+} ILC2s into an ST2^{-} ILC2s phenotype in Si lamina propria at steady state (Fig. 2l). Consistent with previous reports (Yagi et al., 2014), we detected the expression of the serotonin receptor *(Htr1b)* transcript, which was expressed in higher amounts in ILC2^{NAT} compared to ILC2^{INFLAM} (Suppl. Fig. 2d). Since the administration of rIL-33 induced *Tph1* mRNA

expression (Fig. 2a–c), we tested whether *Tph1* mRNA expression at steady state required IL-33 signal. Indeed, *Tph1* mRNA expression was reduced in Si ILC2s sort-purified from *Il33*$^{-/-}$ mice compared to wild-type mice (Fig. 2m). Altogether, these data provide evidence that *Tph1* is specifically expressed in intestinal ILC2s, further up-regulated upon ILC2 activation, and controlled by IL-33.

Tph1 up-regulation in ILC2s upon helminth infection is dependent on IL-33

Next, we tested whether *Tph1* is induced during a physiological type 2 immune response after infection with *N. brasiliensis. Tph1* mRNA expression was strongly up-regulated in ILC2s sorted from mesLN of wild-type mice following *N. brasiliensis* infection, suggesting a potential role for *Tph1* in anti-helminth immunity (Fig. 3a–c). Up-regulation of *Tph1* mRNA expression upon helminth infection was not observed in other lymphocyte populations we examined (Fig. 3d). Given the up-regulation of *Tph1* mRNA expression following ILC2 activation, we then asked whether IL-33 was necessary for the induction of *Tph1* mRNA expression in ILC2s. Unlike wild-type ILC2s, mesLN ILC2s sorted from *Il33*$^{-/-}$ mice failed to up-regulate expression of *Tph1* mRNA following *N. brasiliensis* infection, thus demonstrating the essential role of IL-33 in *Tph1* mRNA regulation (Fig. 3e). These results show that the expression of the gene *Tph1* in ILC2s can be modulated upon *N. brasiliensis* infection and is dependent on IL-33.

Tph1 deletion in lymphocytes results in increased susceptibility to *N. brasiliensis* infection and reduced inflammatory ILC2 response

To further test whether *Tph1* plays a pivotal role in resistance to helminth infection, we generated genetically ablated mice, in which *Tph1* was conditionally deleted in lymphocytes using a Cre recombinase under the *Il7r* promoter (*Il7r*$^{Cre/+}$ *Tph1*$^{flox/flox}$, *Tph1*$^{\Delta/\Delta}$) (Schlenner et al., 2010; Yadav et al., 2008). Consequently, *Tph1* mRNA expression was undetectable in Si ILC2s from *Tph1*$^{\Delta/\Delta}$ mice (Fig. 4a). We also noticed that *Tph1*$^{\Delta/\Delta}$ mice exhibited reduced frequencies of ST2^{-} ILC2s in the Si compared to control mice suggesting that *Tph1* might indeed be involved in the generation of ILC2^{INFLAM} (Fig. 4b,c). Next, we functionally investigated the phenotype of *Tph1*$^{\Delta/\Delta}$ mice using the *N. brasiliensis* infection model. Notably, *Tph1*$^{\Delta/\Delta}$ mice had higher intestinal worm burden compared to their littermate controls on day 7 after infection (Fig. 4d). Since we found that *Tph1* is regulated by IL-33 (Fig. 2a–f and m; Fig. 3a–e), we administered rIL-33 to *Tph1*$^{\Delta/\Delta}$ as well as to *Il33*$^{-/-}$ mice and examined how this affects worm resistance. Administration of exogenous IL-33 to *Tph1*$^{\Delta/\Delta}$ mice rescued their susceptibility to *N. brasiliensis* infection suggesting that *Tph1*-defciency could be overcome by supraphysiological stimulation with rIL-33 (Suppl. Fig. 3a).

To investigate how *Tph1* regulates type 2 immunity, we then analyzed *Tph1*$^{\Delta/\Delta}$ and control mice on day 5 after infection, when the intestinal immune response is triggered. Detailed flow cytometry analysis of mesLN ILC2s revealed that ILC2^{NAT} were present in comparable proportions in *Tph1*$^{\Delta/\Delta}$ mice, whereas ILC2^{INFLAM} cells were reduced on day 5 after infection (Fig. 4e,f). It should be noted that ILC2^{INFLAM} were previously linked to resistance against *N. brasiliensis* infection (Huang et al., 2015; Huang et al., 2018). On day 7 post-infection, ILC2^{INFLAM} were detectable in the mesLN of *Tph1*$^{\Delta/\Delta}$ mice, but were still

reduced compared to control mice (Fig. 4g,h), suggesting a delay in the recruitment to the mesLN rather than a defect in ILC2^{INFLAM} generation. The ILC2^{NAT} response in the mesLN of *Tph1*$^{\Delta/\Delta}$ mice was also affected on day 7 after infection (Fig. 4g,h). However, we did not detect differences in the expression of inflammatory cytokines *Il25* and *Il33* in the intestines of *Tph1*$^{\Delta/\Delta}$ and *Tph1*$^{+/+}$ mice after *N. brasiliensis* infection (Suppl. Fig 3b). In addition, there was a significant negative correlation between ILC2s and worm burden in *Tph1*$^{\Delta/\Delta}$ and control mice (Fig. 4i).

Although T cells expressed very low amounts of *Tph1* mRNA at steady state and after *N. brasiliensis* infection (Fig. 2i and Fig. 3d), we investigated whether *Tph1*$^{\Delta/\Delta}$ mice were still more susceptible to *N. brasiliensis* infection after depletion of CD4$^+$ T cells. Indeed, after treatment with an anti-CD4 depleting antibody, *Tph1*$^{\Delta/\Delta}$ mice had higher worm burden and exhibited decreased ILC2^{INFLAM} response (Fig. 4j–l and Suppl. Fig. 3c,d). Together, these data indicate that *Tph1*-dependent defects in ILC2^{INFLAM} responses occur in the absence of CD4$^+$ T cells and that they are critical for anti-helminth immunity.

To investigate whether this increased parasite susceptibility in *Tph1*$^{\Delta/\Delta}$ mice resulted in a defect in worm clearance, we analyzed worm burden on day 10 after infection, when wild-type mice have completely expelled the parasite (Fig. 4m). Consistent with a defective type 2 immune response, *Tph1*$^{\Delta/\Delta}$ mice failed to expel *N. brasiliensis* on day 10 and still depicted hallmarks of intestinal inflammation measured by lipocalin ELISA (Fig. 4n). Therefore, these data suggest that *Tph1* expression in ILC2s controls ILC2^{INFLAM} expansion following helminth infection, and that *Tph1* is required for the differentiation of ILC2^{NAT} into ILC2^{INFLAM}.

Tph1 deletion leads to defective ILC2 activation

To further uncover the molecular mechanisms by which *Tph1* promotes ILC2 activation and the transition of ILC2^{NAT} into ILC2^{INFLAM}, we performed RNA sequencing (RNA-seq) of sorted Si ILC2s at steady state, and ILC2^{NAT} and ILC2^{INFLAM} from mesenteric lymph nodes on day 7 at the peak of *N. brasiliensis* infection from *Tph1*$^{\Delta/\Delta}$ and control mice. Principal component (PC) analysis plots showed that Si ILC2s, and ILC2^{NAT} and ILC2^{INFLAM} from mesLNs clustered by genotype, and that *Tph1* deletion drove a specific transcriptomic signature (Suppl. Fig. 4a, b). Despite the difference in location, Si ILC2s and mesLN ILC2^{INFLAM} and ILC2^{NAT} shared an array of genes down-regulated in *Tph1*$^{\Delta/\Delta}$ mice (Fig. 5a–d), which were significantly enriched in gene ontology (GO) terms associated with cell division, regulation of cellular component and microtubule-based movements and could be linked to ILC2 activation and migration (Suppl. Fig. 4c–e). Further analysis of the commonly down-regulated genes in *Tph1*$^{\Delta/\Delta}$ from naïve Si ILC2s or mesLN ILC2^{INFLAM} and ILC2^{NAT} from *N. brasiliensis*-infected mice revealed that *Tph1* deletion modulates expression of genes associated with the regulation of immune response, including activating or inhibitory cell surface receptors, such as *Tigit, Cd244* (2B4), *Ctla4* and *Icos* (Fig. 5a–c). Among these genes, inducible T-cell co-stimulator *(Icos)* was of particular interest because it has previously been connected to either ILC2 activation in allergic asthma models or susceptibility to helminth infections (Maazi et al., 2015; Miyahira et al., 2003; Paclik et al., 2015). Reduced *Icos* mRNA and protein expression on Tph1 deficient ILC2s following *N.*

brasiliensis infection was confirmed by qPCR and flow cytometry analyses (Fig. 5e and Suppl. Fig. 4f). Consistent with the role of ICOS in the regulation of ILC2^{INFLAM}, administration of a blocking antibody against ICOS *in vivo* resulted in decreased frequencies of ST2^{-} ILC2s in Si at steady state (Fig. 5f,g). When administered during *N. brasiliensis* infection, treatment with an anti-ICOS blocking antibody caused a decrease in ILC2^{INFLAM} recruitment to the mesLN (Fig. 5h,i). We concluded from these data that ICOS indeed promotes the generation of ILC2^{INFLAM}. Next, to further investigate how Tph1 and ICOS are functionally linked, we treated *Tph1*$^{+/+}$ and *Tph1*$^{\Delta/\Delta}$ mice with a blocking antibody against ICOS following *N. brasiliensis* infection and compared ILC2^{INFLAM} responses in anti-ICOS- or isotype-treated mice from both genotypes. Blocking of ICOS during helminth infection resulted in defective expansion of ILC2^{INFLAM} in *Tph1*$^{+/+}$ mice comparable to that of *Tph1*$^{\Delta/\Delta}$ mice, but had no further effect on ILC2^{INFLAM} recruitment in *Tph1*$^{\Delta/\Delta}$ mice (Fig. 5j). Therefore, these data support a model in which Tph1 regulates ICOS expression in order to promote ILC2^{INFLAM} and anti-helminth immunity. Taken together, we concluded that the delayed and defective ILC2^{INFLAM} responses observed in *Tph1*$^{\Delta/\Delta}$ mice following helminth infection are partially mediated by ICOS.

Discussion

In addition to circulating in the peripheral blood and lymphatics, the multilayered cellular composition of the immune system requires that some immune cell subsets establish permanent tissue residency. Tissue-resident immune cells share common hallmarks, as a sign of tissue residency (Fan and Rudensky, 2016; Klose and Artis, 2016; Rankin and Artis, 2018). While data assessing the whole transcriptome of tissue-resident cells such as ILC2s have been recently published (Bjorklund et al., 2016; Gury-BenAri et al., 2016; Ricardo-Gonzalez et al., 2018; Robinette et al., 2015; Simoni et al., 2017; Yudanin et al., 2019), how tissue-specific cues regulate distinct ILC2 subsets and the associated protective or pathogenic responses remains incompletely defined.

This study provides evidence for a previously unrecognized function of IL-33 and Tph1 in the regulation and the generation of CD25^{-} ST2^{-} ILC2^{INFLAM} from intestine-resident ILC2s, the regulation of ILC2^{INFLAM} and their impact on resistance to worm infections. Although the importance of IL-33 in expulsion of helminth parasites, such as *N. brasiliensis* and *Strongyloides venezuelensis,* is well established (Hung et al., 2013; Moro et al., 2010; Neill et al., 2010; Yasuda et al., 2012), the essential role of IL-33 in promoting ILC2^{INFLAM} responses has not been recognized. To date, IL-25 was the only cytokine reported to be essential for the generation of ILC2^{INFLAM} (Huang et al., 2015) and the current model of ILC2^{INFLAM} differentiation proposes that these cells are constantly generated in the intestine under the control of IL-25 (Huang et al., 2018). Using gain- and loss-of-function approaches, we demonstrated that IL-33 was necessary and sufficient for the induction of ILC2^{INFLAM}. Furthermore, transgenic overexpression of IL-33 in intestinal epithelial cells is sufficient for recruiting ILC2^{INFLAM} to the mesenteric lymph nodes. The finding that both IL-25 and IL-33 were necessary and sufficient to generate ILC2^{INFLAM} responses *in vivo* raises an important question on how these two cytokines act on ILC2s converting them into ILC2^{INFLAM}. It is unlikely that IL-25 alone promotes the generation of ST2^{-} ILC2s *in vivo* since adding IL-25 to ILC2 cultures *in vitro* lead to up-regulation of the IL-33 receptor, ST2;

and a combination of IL-25 and IL-33 together resulted in ST2 down-regulation. The up-regulation of ST2 after *in vitro* stimulation with IL-25 may indicate that the small intestinal $ST2^+$ ILC2s need to receive a second signal, such as IL-33, as a checkpoint to transition into $ILC2^{INFLAM}$ and promote type 2 inflammation. Therefore, we propose a model in which transition of $ILC2^{NAT}$ into $ILC2^{INFLAM}$ is controlled by signals from two distinct parenchymal cells types; IL-25 produced by epithelial tuft cells (Gerbe et al., 2016; Howitt et al., 2016; von Moltke et al., 2016) and now IL-33 presumably derived from intestinal stromal cells (Dahlgren et al., 2019; Kinchen et al., 2018; Mahlakoiv et al., 2019; Rana et al., 2019; Spallanzani et al., 2019). Together, our findings argue that IL-25 and IL-33 are both required and jointly regulate the generation of $ILC2^{INFLAM}$.

Our data support a model where $ILC2^{INFLAM}$ are derived from intestinal ILC2s in the lamina propria, which then migrate to mesenteric lymph nodes upon activation by IL-33, IL-25 and potentially other factors. In accordance with this model, we found that IL-33-dependent intestinal ILC2s had the highest expression of transcript for tryptophan hydroxylase 1 (*Tph1*), the rate-liming enzyme in serotonin biosynthesis, compared to ILC2s derived from other tissues at steady state, suggesting that *Tph1* is a sign of tissue adaptation and regulates transition of small intestinal ILC2s into $ILC2^{INFLAM}$. Taken together, this study provides insights into the alarmin-dependent heterogeneity of ILC2 subsets in tissues and the consequences of this heterogeneity on protective immunity at barrier surfaces.

How immune responses in non-lymphoid tissues, such as mucosal surfaces, are initiated and amplified, but also constrained is poorly understood. To date, the functional consequences of *Tph1* in ILC2s have remained unknown (Robinette et al., 2015; Yagi et al., 2014). Both gain- and loss-of-function experiments at steady state and during helminth infection indictate that *Tph1* expression in ILC2s was tightly contolled by IL-33. Furthermore, we found that the deletion of *Tph1* in lymphocytes resulted in impaired ILC2 responses, decreased type 2 inflammation and increased susceptibility to helminth infection. Mechanistically, we observed that Tph1 deficiency was associated with delayed recruitment of $ILC2^{INFLAM}$ to the mesenteric lymph nodes. Altogether, these data demonstrate a non-redundant role for *Tph1* downstream of IL-33 in driving $ILC2^{INFLAM}$ responses and type 2 immunity. However, administration of rIL-33 could rescue the susceptibility of $Tph1^{\Delta/\Delta}$ mice to *N. brasiliensis* infection. These results suggest that stimulation of type 2 immunity with supraphysiological doses of rIL-33, which is also known to stimulate many other immune cells, including basophils, mast cells and T cells, could overcome Tph1 deficiency and contribute to the rescue of the phenotype observed in $Tph1^{\Delta/\Delta}$ mice (Alvarez et al., 2019; Bonilla et al., 2012; Cohen et al., 2018; Moulin et al., 2007). Recombinant IL-33 administration likely triggers the release of type 2 cytokines from these additional immune cells thus promoting type 2 immunity through *Tph1*-independent mechanisms in other cell types. Our knowledge of the regulators of $ILC2^{INFLAM}$ was limited so far to the alarmin IL-25 and the sphingosine 1-phosphate receptor (Huang et al., 2015; Huang et al., 2018). However, since deleting *Tph1* did not affect *Il25* and *Il33* expression in the intestine after *N. brasiliensis* infection, it is unlikely that *Tph1* directly regulates one of these two alarmins, which promote recruitment of $ILC2^{INFLAM}$. *Tph1* deletion resulted in altered expression of genes associated with the dysregulated immune response, including decreased activating cell surface receptors, such as inducible T-cell co-stimulator *(Icos)*, which has previously been

connected to either ILC2 activation in allergic asthma models or susceptibility to helminth infections (Maazi et al., 2015; Miyahira et al., 2003; Paclik et al., 2015). While our data now show that ICOS is required for the generation of $ILC2^{INFLAM}$ thus providing a cellular mechanism for the failure of worm control, the direct molecular link between Tph1 and ICOS expression regulation requires further investigation.

We demonstrated that the deletion of *Tph1* in lymphocytes results in increased susceptibility to helminth infection and decreased type 2 immunity. Augmented serotonin concentrations have been linked to an enhanced type 2 immune response in allergic asthma (Durk et al., 2013; Lechin et al., 1998), however, the function of serotonin in anti-helminth immunity is poorly understood. Although increased serotonin has been previously reported during worm infections and some studies suggest that serotonin influences immunity against worm infections (Murray et al., 1971; Wang et al., 2018), there is still a gap in knowledge in understanding how serotonin affects type 2 immunity against helminth infections. While it is well established that enterochromaffin cells of the gastrointestinal tract produce the majority of serotonin in the body, our study identifies ILC2s as an additional source of serotonin. Serotonin biology is very complex as serotonin is known to mediate local effects, and the deletion of either peripheral *Tph1* or neuronal *Tph2* results in either pro-inflammatory or anti-inflammatory effects during a colitis model, respectively (Gershon, 2012; Ghia et al., 2009; Margolis et al., 2014). Furthermore, the immune regulation by serotonin probably involves gradients, which are maintained at barrier surfaces. We demonstrated that Tph1 deficiency was associated with delayed recruitment of $ILC2^{INFLAM}$ to the mesenteric lymph nodes, thus, providing a previously unrecognized mechanism for Tph1 to boost anti-helminth immunity. Whereas serotonin receptor agonists and antagonists are now employed for the treatment of functional gastrointestinal disorders, the physiological role of serotonin still remains incompletely understood partly because multiple serotonin receptor subtypes are present in the gut wall (Gershon and Tack, 2007). Serotonin receptors are also widely distributed on many types of immune cells that are recruited following infection by helminth parasites, such as dendritic cells, macrophages, eosinophils and T cells (Herr et al., 2017; Wang et al., 2018). In addition, serotonin has been reported to be a chemotactic gradient factor for cell migration, such as dendritic cells and T cells (Magrini et al., 2011; Muller et al., 2009). $ILC2^{INFLAM}$ were shown to migrate via the lymphatic vessels from the intestine to the mesenteric lymph nodes (Huang et al., 2018). We confirmed that ILC2 express the serotonin receptor *Htr1b*, as previously reported (Yagi et al., 2014) and could sense serotonin. Thus, serotonin could potentially act as an autocrine or paracrine stimulator of ILC2 function or ILC2 migration. Notably, ILC2 have been described to exhibit paracrine or autocrine behavior through ICOS - ICOSL interaction, and IL-9 secretion and sensing via IL-9 receptor expression (Maazi et al., 2015; Miyahira et al., 2003; Paclik et al., 2015; Turner et al., 2013; Wilhelm et al., 2011). Given the role of serotonin in regulating intestinal motility through coordinated actions of the enteric nervous system and muscular contraction via serotonin receptors expression on both cell types (Gershon, 2013; Zeisel et al., 2018), a direct effect on muscle contraction and therefore on worm expulsion cannot be excluded, but also fails to explain the cellular phenotype of $ILC2^{INFLAM}$. Furthermore, ILC2-derived serotonin may have potential receptor-independent effects and may be acting as a post-translational modifier of transcriptional or GTPase activity, a process known as

serotonylation(Farrelly et al., 2019; Walther et al., 2003). Lastly, we cannot exclude an effect of Tph1 and/or serotonin on cell metabolism (Wilhelm et al., 2017).

Collectively, our data identifify a signaling circuit through which alarmins lead to increased transcription of the gene encoding the enzyme tryptophan hydroxylase 1 in lymphocytes to selectively regulate heterogeneity of ILC2 subsets in tissues. Therefore, our study provides insights into the regulation of type 2 immunity at mucosal barriers with potential implications for allergy, immunity to infection and tissue homeostasis.

STAR Methods

Lead Contact and Materials Availability: Lead author: David Artis (dartis@med.cornell.edu)

Mouse strains

Wild-type C57BL/6 mice were purchased from The Jackson Laboratories. *Tph1*$^{fl/fl}$ (Yadav et al., 2008), *Ilr7*$^{Cre/+}$ (Schlenner et al., 2010), *Il33*$^{-/-}$ (provided by Amgen Inc. through Taconic Farms) (Louten et al., 2011), *Vfl33* (He et al., 2018), *Il17rb*$^{-/-}$ (Neill et al., 2010), and *Il1rl1*$^{-/-}$ (Townsend et al., 2000) on a C57BL/6 background, and *Il4*$^{Gfp/Gfp}$ (Mohrs et al., 2001) on a BALB/c background were bred at Weill Cornell Medicine or at Charite. Germ-free on a C57BL/6 background were bred within sterile vinyl isolators at Weill Cornell Gnotobiotic Mouse Facility and monitored for germ-free status by weekly aerobic and anaerobic culturing. Sex and age-matched animals were used for experiments if not otherwise indicated. We did not use randomization to assign animals to experimental groups. No animals were excluded from the analyses. All animal experiments were approved and are in accordance with the local animal care committees.

Isolation of cells from the lamina propria, mesenteric lymph nodes, lung and fat tissue

Small intestine or colon was removed, cleaned from remaining fat tissue and washed in ice-cold PBS (Sigma-Aldrich). Peyer's patches were eliminated, small intestine was opened longitudinally and washed in ice-cold PBS. Dissociation of epithelial cells was performed by incubation on a shaker at 37°C in HBSS (Sigma-Aldrich) containing 10 mM Hepes and 5 mM EDTA (both Thermo Fisher Scientific) or 1 mM DTT (Sigma-Aldrich) two times for 15 min. After each step, samples were vortexed and the epithelial fraction discarded. Afterwards, remaining tissue was chopped into small pieces and enzymatic digestion was performed using 4% FBS, Dispase II (5 U/ml; Thermo Fisher Scientific), Collagenase III (1 mg/ml; Worthington) and DNaseI (0.5 mg/ml; Sigma-Aldrich). Leukocytes were further enriched by Percoll gradient centrifugation (Sigma-Aldrich). Mesenteric lymph nodes were chopped and incubated in RPMI 1640 medium (Sigma-Aldrich) supplemented with 1% BSA (Sigma-Aldrich), Collagenase II (1 mg/ml; Sigma-Aldrich) and DNaseI (20 ng/ml) for 20 min on a shaker at 37°C. Cells were then dissociated using a pasteur pipette, and filtered through a 70 μm cell strainer. Lungs were chopped and incubated in RPMI medium supplemented with Liberase TM (50 μg/ml; Roche) and DNaseI (20 ng/ml) for 1 h at 37°C. The remaining tissues were mashed with a syringe plunger and single cell suspensions were filtered through a 40 μm cell strainer. Leukocytes were then further enriched by 40% Percoll gradient centrifugation and red blood cells were lysed with ACK lysing buffer (Lonza).

Epididymal white adipose tissue was removed and incubated in RPMI medium supplemented with Collagenase II (1 mg/ml), DNaseI (20 ng/ml) for 45 min on a shaker at 37°C and 10 mM EDTA was added for the last 5 min of incubation. After incubation, samples were spun down, the adipocyte layer was aspirated, and the cells were filtered through a 70 μm cell strainer. Mast cells were obtained by lavage of the peritoneal cavity with 10 ml ice cold HBSS supplemented with 1 mM EDTA. For intestinal epithelial cell isolation, intestines were treated as described above and washed in pre-warmed 37°C DMEM (Sigma-Aldrich) with 10% FBS, followed by washes in pre-warmed 37°C PBS, then dissociated in HBSS supplemented with 2 mM EDTA, 1 mM DTT and 5% FBS, filtered through a 100 μm cell strainer, and further enriched by 40%/20% Percoll gradient centrifugation.

Flow cytometry and cell sorting

Dead cells were routinely excluded with Fixable Aqua Dead Cell Stain or SYTOX Blue Dead Cell Stain (both from Thermo Fisher Scientific). Single cell suspensions were incubated on ice with anti-CD16/CD32 (93) antibody (Biolegend) and the following conjugated antibodies in PBS (Ca^{2+} and Mg^{2+}-free, Sigma-Aldrich). Lineage-positive cells were excluded by staining for CD3ε (145-2C11), CD5 (53-7.3), FcεRI (Mar-1), NK1.1 (PK136), NKp46 (29A1.4), B220 (RA3-6B2), CD19 (eBio1D3 (1D3)), CD11b (M1/70) and CD11c (N418). For surface staining the following antibodies were used: KLRG1 (2F1), CD45 (30-F11), CD4 (GK1.5 and RM4-5), CD8α (53-6.7), Sca-1 (D7), c-Kit (2B8), CD25 (PC61), CD127 (A7R34), CCR9 (9B1), CD90.2 (53-2.1), ST2 (DIH9 and RMST2-2), ICOS (7E.17G9), CD326 (G8.8), CD24 (M1/69) and MHC Class II (I-A/I-E) (M5/115.15.2). GATA3 (TWAJ) and Tph1 (EP1311Y, OriGene) were stained using the Foxp3 transcription factor staining buffer set (eBioscience). All antibodies used in flow cytometry were purchased from eBioscience, Biolegend or BD Biosciences if not otherwise indicated. Mast cells were identified as $CD45^+$ Lin^- $FcεR1α^+$ $CD117^+$, intestinal epithelial cells as $CD45^-$ $CD326^+$ $CD24^-$, enterochromaffin cells $CD45^-$ $CD326^+$ $CD24^+$, Treg cells as $CD45^+$ $CD3^+$ $CD4^+$ $CD25^+$ IL-4-GFP^-, Th2 cells as $CD45^+$ $CD3^+$ $CD4^+$ $CD25^-$ IL-4-GFP^+ and mononuclear phagocytes as $CD45^+$ $CD11b^+$ $CD11c^+$ $MHC\text{-}II^+$. All flow cytometry experiments were acquired using a custom configuration Fortessa flow cytometer and the FACS Diva software (BD Biosciences) and analyzed with FlowJo V9.9.3 or V10.4.2 software (TreeStar) or sort-purified by using a custom configuration FACSAria cell sorter (BD Biosciences).

Quantitative real-time PCR

Tissues and sorted cells were homogenized in Trizol (Thermo Fisher Scientific) and stored at −80°C. RNA was extracted with chloroform and RNA concentration was determined using a Nanodrop 2000 spectrophotometer (Thermo Fisher Scientific). Reverse transcription of total RNA was performed using the High Capacity cDNA Reverse Transcription kit according to the protocol provided by the manufacturer (Thermo Fisher Scientific). Reaction was detected on a QuantStudio 6 Flex Real-Time PCR (Thermo Fisher Scientific) using the following TaqMan Gene Expression Assays (Applied Biosystems): Tph1 (Mm01202614_m1), Chga (Mm00514341_m1), Icos (Mm00497600_m1), Cxcr6 (Mm00472858_m1), Tigit (Mm03807522_m1) and Htr1b (Mm00439377_s1) or Sybr green

primers Trim12a (5′ CCTGTCTGTCTGAACCTGATGG 3′ and 5′ GGCTTGAACATTTTGAGCCTCT 3′), Ermn (5′ CTGAGACACTGAGCGGGAC 3′ and 5′ CAACCTTGTAGTATGCCTGGG 3′), Lgmn (5′ TGGACGATCCCGAGGATGG 3′ and 5′ GTGGATGATCTGGTAGGCGT3′), Il25 (QT00134645, Qiagen) and Il33 (QT00135170, Qiagen). Gene expression was normalized as n-fold difference to the housekeeping gene Hprt1 (Mm00446968_m1) or Actb (QT01136772, Qiagen). Relative quantification of gene expression was performed with the QuantStudio Real-Time PCR software version 1.0 (Thermo Fisher Scientific).

Helminth infection and *in vivo* experiments

Third-stage larvae (L3) of *N. brasiliensis* were purified with a Baermann apparatus. After washing three times in PBS, living worms were counted. On day 0, 500 purified worms were injected subcutaneously in PBS. In addition, in some experiments an anti-CD4 depleting antibody (clone GK1.5, 250 μg/mouse, in house) was injected intraperitoneally (i.p.) at day 0 and day 2, 4, and 6 of *N. brasiliensis* infection. In some experiments, anti-ICOS antibody (500 μg/mouse, Bioxcell) and rat IgG isotype control (500 μg/mouse, Sigma-Aldrich) were injected i.p. at day 1 and day 3 of *N. brasiliensis* infection and analyzed on day 5 post-infection, or treated with anti-ICOS antibody or rat IgG isotype control every other day for six days and analyzed one day later. In some experiments, mice were treated with carrier-free recombinant murine IL-33 (1 μg/mouse, R&D Systems) intravenously (i.v.) and analyzed 24 h later or treated with IL-33 (500 ng/mouse) or IL-25 (250μg/mouse, R&D Systems) i.p. for three consecutive days and analyzed one day later. In the IL-33 rescue experiments, mice were injected i.p. with IL-33 (12.5 μg/kg body weight/day) (Brestoff et al., 2015) from day 1 to day 6 of *N. brasiliensis* infection and analyzed 24 h later.

RNA-seq analysis

2,000 ILC2s were sort-purified (Lin$^-$ CD45$^+$ CD127$^+$ KLRG1$^+$) from the lamina propria of the small intestine of naïve *Il7r*$^{Cre/+}$ *Tph1*$^{fl/fl}$ (*Tph1*$^{\Delta/\Delta}$) and *Il7r*$^{Cre/+}$ (*Tph1*$^{+/+}$) control mice or from mesenteric lymph nodes (ILC2^{NAT}: Lin$^-$ CD45$^+$ KLRG1$^+$ ST2$^+$; ILC2^{INFLAM}: Lin$^-$ CD45$^+$ KLRG1$^+$ ST2$^-$) on day 7 after *N. brasiliensis* infection of *Il7r*$^{Cre/+}$ *Tph1*$^{fl/fl}$ (*Tph1*$^{\Delta/\Delta}$) and *Il7r*$^{Cre/+}$ control (*Tph1*$^{+/+}$) mice. Sorted cells in 1x Single-Cell Lysis Buffer (Clontech Laboratories) and Protector RNase Inhibitor (Roche) were used to prepare RNA-seq libraries by the Epigenomics Core at Weill Cornell Medicine using the Clontech SMARTer® Ultra® Low Input RNA Kit V4 (Clontech Laboratories). Sequencing was performed on an Illumina HiSeq 2500 (Illumina), yielding 50 bp single-end reads. Raw sequencing reads were demultiplexed with Illumina CASAVA (v2.17). Adapters were trimmed from reads using FLEXBAR (v2.4) (Dodt et al., 2012) and reads were aligned to the NCBI GRCm38/mm10 mouse genome using the STAR aligner (v2.3.0) (Dobin et al., 2013) with default settings. Small intestinal ILC2s from PBS- and IL-33-treated mice (Fig. 2a,b) were sort-purified as previously described (Klose et al., 2017). RNA-seq libraries from small intestinal ILC2s of IL33-treated mice (Fig. 2a,b) were previously sequenced together with those from PBS-treated mice. Raw sequence data from the PBS-treated mice are available on the Gene Expression Omnibus (GEO) under the series GSE101625 (Klose et al., 2017), which also includes sequence data from small intestinal ILC2s and ILC3s from SPF mice (Fig. 2h). ILC2s from mesLN of naïve and *N. brasiliensis*-infected mice (Fig.

3a,b) were sort-purified as previously described (Moriyama et al., 2018). Raw RNA-seq data from mesLN ILC2s of naïve mice (Fig. 3a,b) were generated simultaneously with those from *N. brasiliensis*-infected mice, which have previously been made available through the GEO accession GSE108884 (Moriyama et al., 2018). Read counts per gene (RefSeq annotation) were determined using the Rsubread R package (Liao et al., 2013). One $ILC2^{NAT}$ sample from the $Tph1^{\Delta/\Delta}$ group was excluded from the analysis (Fig. 5c and Suppl. Fig. 4b,e) because its library size was anomalously small (fewer than 1000 mapped reads). Prior to differential expression analysis, genes were prefiltered, keeping only genes with at least 50 mapped reads in at least 2 samples. Differential expression analysis was performed using DESeq2 version 1.20.0 with default parameters and with a false discovery rate (FDR) of 0.1 (Love et al., 2014). Principal component analysis was performed after using DESeq2's variance stabilizing transformation. Gene Ontology enrichment analysis was performed using the enrichGO function of the clusterProfiler R package (Yu et al., 2012) with the Biological Process (BP) ontology and using as background the set of all genes that passed DESeq2's independent filtering function (that is, all genes that were assigned an adjusted p value by DESeq2). The resulting p values were adjusted to yield false discovery rates (FDR) with FDR < 0.1 taken to indicate significance.

Lipocalin-2 ELISA

For Lipocalin-2 ELISA, 2-3 fecal pellets from each mouse were collected, frozen and stored at −80°C until processed. Collected fecal material was homogenized in 500 μl PBS and fecal debris was eliminated by centrifugation at 10,000g for 5 min. The concentration of soluble Lipocalin-2 in the fecal supernatants was quantified using the Lipocalin-2/NGAL DuoSet ELISA system according to the manufacturers recommendations (R&D Systems).

Serotonin ELISA

Sort-purified small intestinal ILC2s were incubated in RPMI supplemented with 10% FCS previously treated with dextran-coated charcoal (0.25% wt/vol, Sigma-Aldrich) to absorb exogenous serotonin, 25 mM Hepes, 1 mM sodium pyruvate, 55 μM 2-Mercaptoethanol, 1x MEM non-essential amino acid solution, 2 mM L-Glutamine, 100 U/ml Penicillin and 100 μg/ml Streptomycin (all Gibco) in 96-well microtiter plates (Nunc) for 4 days at 37°C and 5% CO_2, in the presence of IL-2, IL-7 (both at 10 ng/ml, R&D Systems), IL-33 (30 ng/ml, R&D Systems) and 30 μm tranylcypromine hemisulfate (Focus Biomolecules). Serotonin released into culture supernatants was quantified using the Ultra Sensitive Serotonin enzyme immunoassay (EIA, Labor Diagnostika Nord), according to the manufacture's protocol.

In vitro culture

Sort-purified intestinal ILC2s were cultured in DMEM with high glucose supplemented with 10% FBS, 10 mM Hepes, 1 mM sodium pyruvate, 1x MEM non-essential amino acid solution, 80 μM 2-Mercaptoethanol, 2 mM L-Glutamine, 100 U/ml Penicillin and 100 μg/ml Streptomycin in 96-well microtiter plates at 37°C and 5% CO_2 for 3 days, in the presence of IL-7, IL-25 and IL-33 (20 ng/ml each, all from Biolegend) as indicated.

Immunofluorescence microscopy

Intestine was fixed in 2% paraformaldehyde in PBS (Electron Microscopy Sciences) for 2 h on ice and incubated in 30% sucrose at 4°C overnight, followed by embedding in tissue freezing medium OCT (Leica) for cryocutting. 6 μm slices were prepared on microscopy slides, washed 3x in ice-cold PBS, blocked in 10% BSA, 0.3% Triton X-100 (Sigma-Aldrich) in PBS, treated with the Streptavidin/Biotin blocking kit (Vector laboratories) and stained. The following antibodies were used: mouse anti-serotonin (5HT-H209, Dako), hamster anti-CD3ε (eBio500A2, biotinylated, eBioscience), hamster anti-KLRG1 (2F1, PE, eBioscience), streptavidin (Alexa Fluor 647, BioLegend) , polyclonal goat anti-mouse IL-33 (R&D Systems), E-Cadherin (36/E-Cadherin, BD Pharmingen), donkey anti-goat IgG (Thermo Fisher Scientific) and goat anti-mouse IgG1 (Thermo Fisher Scientific). Nuclei were counterstain with DAPI (Thermo Fisher Scientific). Representative images were captured under an inverted Nikon Eclipse Ti microscope (Nikon).

Statistical analysis

P value of data sets was determined by paired or unpaired two-tailed Student's t-test with 95% confidence interval. Normal distribution was assumed. If equal variances between two groups could not be assumed, Welch's correction was performed. Difference in lipocalin-2 concentrations between two groups were assessed by a non-parametric Mann-Whitney test. The Spearman rank order correlation test was used to analyze correlation. All statistical tests were performed with Graph Pad Prism V7 software (GraphPad Software, Inc.). (*p <0.05; **p <0.01; ***p <0.001; ****p <0.0001 and n.s., not significant). Investigators were not blinded to group allocation during experiments.

Data availability

RNA-seq data is deposited in the GEO repository database under the series GSE145289.

Supplementary Material

Refer to Web version on PubMed Central for supplementary material.

Acknowledgments

We thank the members of the Artis lab for critically reading the manuscript and the epigenomics core at Weill Cornell Medicine for carrying out the RNA sequencing, The work was supported by grants from the German Research Foundation (DFG; KL 2963/1-1 and KL 2963/2-1 to C.S.N.K. and SFB 873-B11to H.-R.R.), the European Research Council (Starting Grant 803087 to C.S.N.K. and Advanced Grant 742883 to H.-R.R.), the Novo Nordic Foundation (14052 to J.B.M.), NIH fellowship (F32AI124517 to N.J.B), JSPS Overseas Research Fellowships (to S.M.), the National Institutes of Health (NIH; AI074878, AI095466, AI095608 and AI102942 to D.A., and 2P01AG032959-09 to G.K.), the Burroughs Wellcome Fund (to D.A.) and the Crohn's & Colitis Foundation of America (to T.M. and D.A.), Cure for IBD (to D.A.) and the Rosanne H. Silberman Foundation (to D.A.).

References

Alvarez F, Fritz JH, and Piccirillo CA (2019). Pleiotropic Effects of IL-33 on CD4(+) T Cell Differentiation and Effector Functions. Frontiers in immunology 10, 522. [PubMed: 30949175]

Artis D, and Spits H (2015). The biology of innate lymphoid cells. Nature 517, 293–301. [PubMed: 25592534]

Bjorklund AK, Forkel M, Picelli S, Konya V, Theorell J, Friberg D, Sandberg R, and Mjosberg J (2016). The heterogeneity of human CD127(+) innate lymphoid cells revealed by single-cell RNA sequencing. Nature immunology 17, 451–460. [PubMed: 26878113]

Bonilla WV, Frohlich A, Senn K, Kallert S, Fernandez M, Johnson S, Kreutzfeldt M, Hegazy AN, Schrick C, Fallon PG, et al. (2012). The alarmin interleukin-33 drives protective antiviral CD8(+) T cell responses. Science 335, 984–989. [PubMed: 22323740]

Brestoff JR, Kim BS, Saenz SA, Stine RR, Monticelli LA, Sonnenberg GF, Thome JJ, Farber DL, Lutfy K, Seale P, and Artis D (2015). Group 2 innate lymphoid cells promote beiging of white adipose tissue and limit obesity. Nature 519, 242–246. [PubMed: 25533952]

Cohen M, Giladi A, Gorki AD, Solodkin DG, Zada M, Hladik A, Miklosi A, Salame TM, Halpern KB, David E, et al. (2018). Lung Single-Cell Signaling Interaction Map Reveals Basophil Role in Macrophage Imprinting. Cell 175, 1031–1044 e1018. [PubMed: 30318149]

Dahlgren MW, Jones SW, Cautivo KM, Dubinin A, Ortiz-Carpena JF, Farhat S, Yu KS, Lee K, Wang C, Molofsky AV, et al. (2019). Adventitial Stromal Cells Define Group 2 Innate Lymphoid Cell Tissue Niches. Immunity 50, 707–722 e706. [PubMed: 30824323]

Diefenbach A, Colonna M, and Koyasu S (2014). Development, differentiation, and diversity of innate lymphoid cells. Immunity 41, 354–365. [PubMed: 25238093]

Dobin A, Davis CA, Schlesinger F, Drenkow J, Zaleski C, Jha S, Batut P, Chaisson M, and Gingeras TR (2013). STAR: ultrafast universal RNA-seq aligner. Bioinformatics 29, 15–21. [PubMed: 23104886]

Dodt M, Roehr JT, Ahmed R, and Dieterich C (2012). FLEXBAR-Flexible Barcode and Adapter Processing for Next-Generation Sequencing Platforms. Biology 1, 895–905. [PubMed: 24832523]

Durk T, Duerschmied D, Muller T, Grimm M, Reuter S, Vieira RP, Ayata K, Cicko S, Sorichter S, Walther DJ, et al. (2013). Production of serotonin by tryptophan hydroxylase 1 and release via platelets contribute to allergic airway inflammation. American journal of respiratory and critical care medicine 187, 476–485. [PubMed: 23328530]

Eberl G, Colonna M, Di Santo JP, and McKenzie AN (2015). Innate lymphoid cells Innate lymphoid cells: a new paradigm in immunology. Science 348, aaa6566. [PubMed: 25999512]

Fan X, and Rudensky AY (2016). Hallmarks of Tissue-Resident Lymphocytes. Cell 164, 1198–1211. [PubMed: 26967286]

Farrelly LA, Thompson RE, Zhao S, Lepack AE, Lyu Y, Bhanu NV, Zhang B, Loh YE, Ramakrishnan A, Vadodaria KC, et al. (2019). Histone serotonylation is a permissive modification that enhances TFIID binding to H3K4me3. Nature 567, 535–539. [PubMed: 30867594]

Gasteiger G, Fan X, Dikiy S, Lee SY, and Rudensky AY (2015). Tissue residency of innate lymphoid cells in lymphoid and nonlymphoid organs. Science 350, 981–985. [PubMed: 26472762]

Gerbe F, Sidot E, Smyth DJ, Ohmoto M, Matsumoto I, Dardalhon V, Cesses P, Garnier L, Pouzolles M, Brulin B, et al. (2016). Intestinal epithelial tuft cells initiate type 2 mucosal immunity to helminth parasites. Nature 529, 226–230. [PubMed: 26762460]

Gershon MD (2012). Serotonin is a sword and a shield of the bowel: serotonin plays offense and defense. Trans Am Clin Climatol Assoc 123, 268–280; discussion 280. [PubMed: 23303993]

Gershon MD (2013). 5-Hydroxytryptamine (serotonin) in the gastrointestinal tract. Curr Opin Endocrinol Diabetes obes 20, 14–21. [PubMed: 23222853]

Gershon MD, and Tack J (2007). The serotonin signaling system: from basic understanding to drug development for functional GI disorders. Gastroenterology 132, 397–414. [PubMed: 17241888]

Ghia JE, Li N, Wang H, Collins M, Deng Y, El-Sharkawy RT, Cote F, Mallet J, and Khan WI (2009). Serotonin has a key role in pathogenesis of experimental colitis. Gastroenterology 137, 1649–1660. [PubMed: 19706294]

Gury-BenAri M, Thaiss CA, Serafini N, Winter DR, Giladi A, Lara-Astiaso D, Levy M, Salame TM, Weiner A, David E, et al. (2016). The Spectrum and Regulatory Landscape of Intestinal Innate Lymphoid Cells Are Shaped by the Microbiome. Cell 166, 1231–1246 e1213. [PubMed: 27545347]

Halim TY, Krauss RH, Sun AC, and Takei F (2012). Lung natural helper cells are a critical source of Th2 cell-type cytokines in protease allergen-induced airway inflammation. Immunity 36, 451–463. [PubMed: 22425247]

Halim TY, Steer CA, Matha L, Gold MJ, Martinez-Gonzalez I, McNagny KM, McKenzie AN, and Takei F (2014). Group 2 innate lymphoid cells are critical for the initiation of adaptive T helper 2 cell-mediated allergic lung inflammation. Immunity 40, 425–435. [PubMed: 24613091]

He Z, Chen L, Furtado GC, and Lira SA (2018). Interleukin 33 regulates gene expression in intestinal epithelial cells independently of its nuclear localization. Cytokine 111, 146–153. [PubMed: 30145369]

Herr N, Bode C, and Duerschmied D (2017). The Effects of Serotonin in Immune Cells. Front Cardiovasc Med 4, 48. [PubMed: 28775986]

Howitt MR, Lavoie S, Michaud M, Blum AM, Tran SV, Weinstock JV, Gallini CA, Redding K, Margolskee RF, Osborne LC, et al. (2016). Tuft cells, taste-chemosensory cells, orchestrate parasite type 2 immunity in the gut. Science 351, 1329–1333. [PubMed: 26847546]

Hoyler T, Klose CS, Souabni A, Turqueti-Neves A, Pfeifer D, Rawlins EL, Voehringer D, Busslinger M, and Diefenbach A (2012). The Transcription Factor GATA-3 Controls Cell Fate and Maintenance of Type 2 Innate Lymphoid Cells. Immunity 37, 634–648. [PubMed: 23063333]

Huang Y, Guo L, Qiu J, Chen X, Hu-Li J, Siebenlist U, Williamson PR, Urban JF Jr., and Paul WE (2015). IL-25-responsive, lineage-negative KLRG1(hi) cells are multipotential 'inflammatory' type 2 innate lymphoid cells. Nature immunology 16, 161–169. [PubMed: 25531830]

Huang Y, Mao K, Chen X, Sun MA, Kawabe T, Li W, Usher N, Zhu J, Urban JF Jr., Paul WE, and Germain RN (2018). S1P-dependent interorgan trafficking of group 2 innate lymphoid cells supports host defense. Science 359, 114–119. [PubMed: 29302015]

Hung LY, Lewkowich IP, Dawson LA, Downey J, Yang Y, Smith DE, and Herbert D R. (2013). IL-33 drives biphasic IL-13 production for noncanonical Type 2 immunity against hookworms. Proceedings of the National Academy of Sciences of the United States of America 110, 282–287. [PubMed: 23248269]

Imai Y, Yasuda K, Sakaguchi Y, Haneda T, Mizutani H, Yoshimoto T, Nakanishi K, and Yamanishi K (2013). Skin-specific expression of IL-33 activates group 2 innate lymphoid cells and elicits atopic dermatitis-like inflammation in mice. Proceedings of the National Academy of Sciences of the United States of America 110, 13921–13926. [PubMed: 23918359]

Kim BS, Siracusa MC, Saenz SA, Noti M, Monticelli LA, Sonnenberg GF, Hepworth MR, Van Voorhees AS, Comeau MR, and Artis D (2013). TSLP elicits IL-33-independent innate lymphoid cell responses to promote skin inflammation. Science translational medicine 5, 170ra116.

Kinchen J, Chen HH, Parikh K, Antanaviciute A, Jagielowicz M, Fawkner-Corbett D, Ashley N, Cubitt L, Mellado-Gomez E, Attar M, et al. (2018). Structural Remodeling of the Human Colonic Mesenchyme in Inflammatory Bowel Disease. Cell 175, 372–386 e317. [PubMed: 30270042]

Klose CS, and Artis D (2016). Innate lymphoid cells as regulators of immunity, inflammation and tissue homeostasis. Nature immunology 17, 765–774. [PubMed: 27328006]

Klose CSN, Mahlakoiv T, Moeller JB, Rankin LC, Flamar AL, Kabata H, Monticelli LA, Moriyama S, Putzel GG, Rakhilin N, et al. (2017). The neuropeptide neuromedin U stimulates innate lymphoid cells and type 2 inflammation. Nature 549, 282–286. [PubMed: 28869965]

Lechin F, van der Dijs B, Orozco B, Jara H, Rada I, Lechin ME, and Lechin AE (1998). The serotonin uptake-enhancing drug tianeptine suppresses asthmatic symptoms in children: a double-blind, crossover, placebo-controlled study. Journal of clinical pharmacology 38, 918–925. [PubMed: 9807972]

Li J, Zhang Y, and Zhang L (2015). Discovering susceptibility genes for allergic rhinitis and allergy using a genome-wide association study strategy. Current opinion in allergy and clinical immunology 15, 33–40. [PubMed: 25304232]

Liao Y, Smyth GK, and Shi W (2013). The Subread aligner: fast, accurate and scalable read mapping by seed-and-vote. Nucleic acids research 41, e108. [PubMed: 23558742]

Louten J, Rankin AL, Li Y, Murphy EE, Beaumont M, Moon C, Bourne P, McClanahan TK, Pflanz S, and de Waal Malefyt R (2011). Endogenous IL-33 enhances Th2 cytokine production and T-cell responses during allergic airway inflammation. Int Immunol 23, 307–315. [PubMed: 21422152]

Love MI, Huber W, and Anders S (2014). Moderated estimation of fold change and dispersion for RNA-seq data with DESeq2. Genome biology 15, 550. [PubMed: 25516281]

Lund ML, Egerod KL, Engelstoft MS, Dmytriyeva O, Theodorsson E, Patel BA, and Schwartz TW (2018). Enterochromaffin 5-HT cells - A major target for GLP-1 and gut microbial metabolites. Mol Metab 11, 70–83. [PubMed: 29576437]

Maazi H, Patel N, Sankaranarayanan I, Suzuki Y, Rigas D, Soroosh P, Freeman GJ, Sharpe AH, and Akbari O (2015). ICOS:ICOS-ligand interaction is required for type 2 innate lymphoid cell function, homeostasis, and induction of airway hyperreactivity. Immunity 42, 538–551. [PubMed: 25769613]

Magrini E, Szabo I, Doni A, Cibella J, and Viola A (2011). Serotonin-mediated tuning of human helper T cell responsiveness to the chemokine CXCL12. PloS one 6, e22482. [PubMed: 21853036]

Mahlakoiv T, Flamar AL, Johnston LK, Moriyama S, Putzel GG, Bryce PJ, and Artis D (2019). Stromal cells maintain immune cell homeostasis in adipose tissue via production of interleukin-33. Sci Immunol 4.

Margolis KG, Stevanovic K, Li Z, Yang QM, Oravecz T, Zambrowicz B, Jhaver KG, Diacou A, and Gershon MD (2014). Pharmacological reduction of mucosal but not neuronal serotonin opposes inflammation in mouse intestine. Gut 63, 928–937. [PubMed: 23749550]

McHedlidze T, Waldner M, Zopf S, Walker J, Rankin AL, Schuchmann M, Voehringer D, McKenzie AN, Neurath MF, Pflanz S, and Wirtz S (2013). Interleukin-33-dependent innate lymphoid cells mediate hepatic fibrosis. Immunity 39, 357–371. [PubMed: 23954132]

Miyahira Y, Akiba H, Ogawa SH, Ishi T, Watanabe S, Kobayashi S, Takeuchi T, Aoki T, Tezuka K, Abe R, et al. (2003). Involvement of ICOS-B7RP-1 costimulatory pathway in the regulation of immune responses to Leishmania major and Nippostrongylus brasiliensis infections. Immunology letters 89, 193–199. [PubMed: 14556978]

Mjosberg J, Bernink J, Golebski K, Karrich JJ, Peters CP, Blom B, Te Velde AA, Fokkens WJ, van Drunen CM, and Spits H (2012). The Transcription Factor GATA3 Is Essential for the Function of Human Type 2 Innate Lymphoid Cells. Immunity 37, 649–659. [PubMed: 23063330]

Moffatt MF, Gut IG, Demenais F, Strachan DP, Bouzigon E, Heath S, von Mutius E , Farrall M, Lathrop M, and Cookson W (2010). A large-scale, consortium-based genomewide association study of asthma. The New England journal of medicine 363, 1211–1221. [PubMed: 20860503]

Mohrs M, Shinkai K, Mohrs K, and Locksley RM (2001). Analysis of type 2 immunity in vivo with a bicistronic IL-4 reporter. Immunity 15, 303–311. [PubMed: 11520464]

Molofsky AB, Savage AK, and Locksley RM (2015a). Interleukin-33 in Tissue Homeostasis, Injury, and Inflammation. Immunity 42, 1005–1019. [PubMed: 26084021]

Molofsky AB, Van Gool F, Liang HE, Van Dyken SJ, Nussbaum JC, Lee J, Bluestone JA, and Locksley RM (2015b). Interleukin-33 and Interferon-gamma Counter-Regulate Group 2 Innate Lymphoid Cell Activation during Immune Perturbation. Immunity 43, 161–174. [PubMed: 26092469]

Monticelli LA, Osborne LC, Noti M, Tran SV, Zaiss DM, and Artis D (2015). IL-33 promotes an innate immune pathway of intestinal tissue protection dependent on amphiregulin-EGFR interactions. Proceedings of the National Academy of Sciences of the United States of America 112, 10762–10767. [PubMed: 26243875]

Monticelli LA, Sonnenberg GF, Abt MC, Alenghat T, Ziegler CG, Doering TA, Angelosanto JM, Laidlaw BJ, Yang CY, Sathaliyawala T, et al. (2011). Innate lymphoid cells promote lung-tissue homeostasis after infection with influenza virus. Nature immunology 12, 1045–1054. [PubMed: 21946417]

Moriyama S, Brestoff JR, Flamar AL, Moeller JB, Klose CSN, Rankin LC, Yudanin NA, Monticelli LA, Putzel GG, Rodewald HR, and Artis D (2018). beta2-adrenergic receptor-mediated negative regulation of group 2 innate lymphoid cell responses. Science 359, 1056–1061. [PubMed: 29496881]

Moro K, Kabata H, Tanabe M, Koga S, Takeno N, Mochizuki M, Fukunaga K, Asano K, Betsuyaku T, and Koyasu S (2016). Interferon and IL-27 antagonize the function of group 2 innate lymphoid cells and type 2 innate immune responses. Nature immunology 17, 76–86. [PubMed: 26595888]

Moro K, Yamada T, Tanabe M, Takeuchi T, Ikawa T, Kawamoto H, Furusawa J, Ohtani M, Fujii H, and Koyasu S (2010). Innate production of T(H)2 cytokines by adipose tissue-associated c-Kit(+)Sca-1(+) lymphoid cells. Nature 463, 540–544. [PubMed: 20023630]

Moulin D, Donze O, Talabot-Ayer D, Mezin F, Palmer G, and Gabay C (2007). Interleukin (IL)-33 induces the release of pro-inflammatory mediators by mast cells. Cytokine 40, 216–225. [PubMed: 18023358]

Muller T, Durk T, Blumenthal B, Grimm M, Cicko S, Panther E, Sorichter S, Herouy Y, Di Virgilio F, Ferrari D, et al. (2009). 5-hydroxytryptamine modulates migration, cytokine and chemokine release and T-cell priming capacity of dendritic cells in vitro and in vivo. PloS one 4, e6453. [PubMed: 19649285]

Murray M, Smith WD, Waddell AH, and Jarrett WF (1971). Nippostrongylus brasiliensis: histamine and 5-hydroxytryptamine inhibition and worm expulsion. Experimental parasitology 30, 58–63. [PubMed: 4400480]

Nagashima H, Okuyama Y, Fujita T, Takeda T, Motomura Y, Moro K, Hidaka T, Omori K, Sakurai T, Machiyama T, et al. (2018). GITR cosignal in ILC2s controls allergic lung inflammation. The Journal of allergy and clinical immunology 141, 1939–1943 e1938. [PubMed: 29427641]

Neill DR, Wong SH, Bellosi A, Flynn RJ, Daly M, Langford TK, Bucks C, Kane CM, Fallon PG, Pannell R, et al. (2010). Nuocytes represent a new innate effector leukocyte that mediates type-2 immunity. Nature 464, 1367–1370. [PubMed: 20200518]

Nowak EC, de Vries VC, Wasiuk A, Ahonen C, Bennett KA, Le Mercier I, Ha DG, and Noelle RJ (2012). Tryptophan hydroxylase-1 regulates immune tolerance and inflammation. The Journal of experimental medicine 209, 2127–2135. [PubMed: 23008335]

Paclik D, Stehle C, Lahmann A, Hutloff A, and Romagnani C (2015). ICOS regulates the pool of group 2 innate lymphoid cells under homeostatic and inflammatory conditions in mice. European journal of immunology 45, 2766–2772. [PubMed: 26249010]

Peng H, Jiang X, Chen Y, Sojka DK, Wei H, Gao X, Sun R, Yokoyama WM, and Tian Z (2013). Liver-resident NK cells confer adaptive immunity in skin-contact inflammation. The Journal of clinical investigation 123, 1444–1456. [PubMed: 23524967]

Price AE, Liang HE, Sullivan BM, Reinhardt RL, Eisley CJ, Erle DJ, and Locksley RM (2010). Systemically dispersed innate IL-13-expressing cells in type 2 immunity. Proceedings of the National Academy of Sciences of the United States of America 107, 11489–11494. [PubMed: 20534524]

Rak GD, Osborne LC, Siracusa MC, Kim BS, Wang K, Bayat A, Artis D, and Volk SW (2016). IL-33-Dependent Group 2 Innate Lymphoid Cells Promote Cutaneous Wound Healing. The Journal of investigative dermatology 136, 487–496. [PubMed: 26802241]

Rana BMJ, Jou E, Barlow JL, Rodriguez-Rodriguez N, Walker JA, Knox C, Jolin HE, Hardman CS, Sivasubramaniam M, Szeto A, et al. (2019). A stromal cell niche sustains ILC2-mediated type-2 conditioning in adipose tissue. The Journal of experimental medicine 216, 1999–2009. [PubMed: 31248899]

Rankin LC, and Artis D (2018). Beyond Host Defense: Emerging Functions of the Immune System in Regulating Complex Tissue Physiology. Cell 173, 554–567. [PubMed: 29677509]

Ricardo-Gonzalez RR, Van Dyken SJ, Schneider C, Lee J, Nussbaum JC, Liang HE, Vaka D, Eckalbar WL, Molofsky AB, Erle DJ, and Locksley RM (2018). Tissue signals imprint ILC2 identity with anticipatory function. Nature immunology.

Ringvall M, Ronnberg E, Wernersson S, Duelli A, Henningsson F, Abrink M, Garcia-Faroldi G, Fajardo I, and Pejler G (2008). Serotonin and histamine storage in mast cell secretory granules is dependent on serglycin proteoglycan. The Journal of allergy and clinical immunology 121, 1020–1026. [PubMed: 18234316]

Robinette ML, Fuchs A, Cortez VS, Lee JS, Wang Y, Durum SK, Gilfillan S, Colonna M, and Immunological Genome C (2015). Transcriptional programs define molecular characteristics of innate lymphoid cell classes and subsets. Nature immunology 16, 306–317. [PubMed: 25621825]

Salimi M, Barlow JL, Saunders SP, Xue L, Gutowska-Owsiak D, Wang X, Huang LC, Johnson D, Scanlon ST, McKenzie AN, et al. (2013). A role for IL-25 and IL-33-driven type-2 innate

lymphoid cells in atopic dermatitis. The Journal of experimental medicine 210, 2939–2950. [PubMed: 24323357]

Schlenner SM, Madan V, Busch K, Tietz A, Laufle C, Costa C, Blum C, Fehling HJ, and Rodewald HR (2010). Fate mapping reveals separate origins of T cells and myeloid lineages in the thymus. Immunity 32, 426–436. [PubMed: 20303297]

Simoni Y, Fehlings M, Kloverpris HN, McGovern N, Koo SL, Loh CY, Lim S, Kurioka A, Fergusson JR, Tang CL, et al. (2017). Human Innate Lymphoid Cell Subsets Possess Tissue-Type Based Heterogeneity in Phenotype and Frequency. Immunity 46, 148–161. [PubMed: 27986455]

Spallanzani RG, Zemmour D, Xiao T, Jayewickreme T, Li C, Bryce PJ, Benoist C, and Mathis D (2019). Distinct immunocyte-promoting and adipocyte-generating stromal components coordinate adipose tissue immune and metabolic tenors. Sci Immunol 4.

Spits H, Artis D, Colonna M, Diefenbach A, Di Santo JP, Eberl G, Koyasu S, Locksley RM, McKenzie AN, Mebius RE, et al. (2013). Innate lymphoid cells - a proposal for uniform nomenclature. Nature reviews. Immunology 13, 145–149.

Townsend MJ, Fallon PG, Matthews DJ, Jolin HE, and McKenzie AN (2000). T1/ST2-deficient mice demonstrate the importance of T1/ST2 in developing primary T helper cell type 2 responses. The Journal of experimental medicine 191, 1069–1076. [PubMed: 10727469]

Turner JE, Morrison PJ, Wilhelm C, Wilson M, Ahlfors H, Renauld JC, Panzer U, Helmby H, and Stockinger B (2013). IL-9-mediated survival of type 2 innate lymphoid cells promotes damage control in helminth-induced lung inflammation. The Journal of experimental medicine 210, 2951–2965. [PubMed: 24249111]

Vivier E, Artis D, Colonna M, Diefenbach A, Di Santo JP, Eberl G, Koyasu S, Locksley RM, McKenzie ANJ, Mebius RE, et al. (2018). Innate Lymphoid Cells: 10 Years On. Cell 174, 1054–1066. [PubMed: 30142344]

von Moltke J, Ji M, Liang HE, and Locksley RM (2016). Tuft-cell-derived IL-25 regulates an intestinal ILC2-epithelial response circuit. Nature 529, 221–225. [PubMed: 26675736]

Walther DJ, Peter JU, Winter S, Holtje M, Paulmann N, Grohmann M, Vowinckel J, Alamo-Bethencourt V, Wilhelm CS, Ahnert-Hilger G, and Bader M (2003). Serotonylation of small GTPases is a signal transduction pathway that triggers platelet alpha-granule release. Cell 115, 851–862. [PubMed: 14697203]

Wang SJ, Sharkey KA, and McKay DM (2018). Modulation of the immune response by helminths: a role for serotonin? Bioscience reports 38.

Wilhelm C, Hirota K, Stieglitz B, Van Snick J, Tolaini M, Lahl K, Sparwasser T, Helmby H, and Stockinger B (2011). An IL-9 fate reporter demonstrates the induction of an innate IL-9 response in lung inflammation. Nature immunology 12, 1071–1077. [PubMed: 21983833]

Wilhelm C, Kharabi Masouleh S, and Kazakov A (2017). Metabolic Regulation of Innate Lymphoid Cell-Mediated Tissue Protection-Linking the Nutritional State to Barrier Immunity. Frontiers in immunology 8, 1742. [PubMed: 29375541]

Yadav VK, Ryu JH, Suda N, Tanaka KF, Gingrich JA, Schutz G, Glorieux FH, Chiang CY, Zajac JD, Insogna KL, et al. (2008). Lrp5 controls bone formation by inhibiting serotonin synthesis in the duodenum. Cell 135, 825–837. [PubMed: 19041748]

Yagi R, Zhong C, Northrup DL, Yu F, Bouladoux N, Spencer S, Hu G, Barron L, Sharma S, Nakayama T, et al. (2014). The Transcription Factor GATA3 Is Critical for the Development of All IL-7Ralpha-Expressing Innate Lymphoid Cells. Immunity 40, 378–388. [PubMed: 24631153]

Yasuda K, Muto T, Kawagoe T, Matsumoto M, Sasaki Y, Matsushita K, Taki Y, Futatsugi-Yumikura S, Tsutsui H, Ishii KJ, et al. (2012). Contribution of IL-33-activated type II innate lymphoid cells to pulmonary eosinophilia in intestinal nematode-infected mice. Proceedings of the National Academy of Sciences of the United States of America 109, 3451–3456. [PubMed: 22331917]

Yu G, Wang LG, Han Y, and He QY (2012). clusterProfiler: an R package for comparing biological themes among gene clusters. OMICS 16, 284–287. [PubMed: 22455463]

Yudanin NA, Schmitz F, Flamar AL, Thome JJC, Tait Wojno E, Moeller JB, Schirmer M, Latorre IJ, Xavier RJ, Farber DL, et al. (2019). Spatial and Temporal Mapping of Human Innate Lymphoid Cells Reveals Elements of Tissue Specificity. Immunity 50, 505–519 e504. [PubMed: 30770247]

Zeisel A, Hochgerner H, Lonnerberg P, Johnsson A, Memic F, van der Zwan J, Haring M, Braun E, Borm LE, La Manno G, et al. (2018). Molecular Architecture of the Mouse Nervous System. Cell 174, 999–1014 e1022. [PubMed: 30096314]

Highlights:

- IL-33 promotes inflammatory ILC2s
- Tph1 is up-regulated in ILC2s upon activation in an IL-33-dependent manner
- *Il7r*$^{Cre/+}$ *Tph1*$^{flox/flox}$ mice are highly susceptible to helminth infections
- *Tph1* regulates inflammatory ILC2 responses during helminth infection

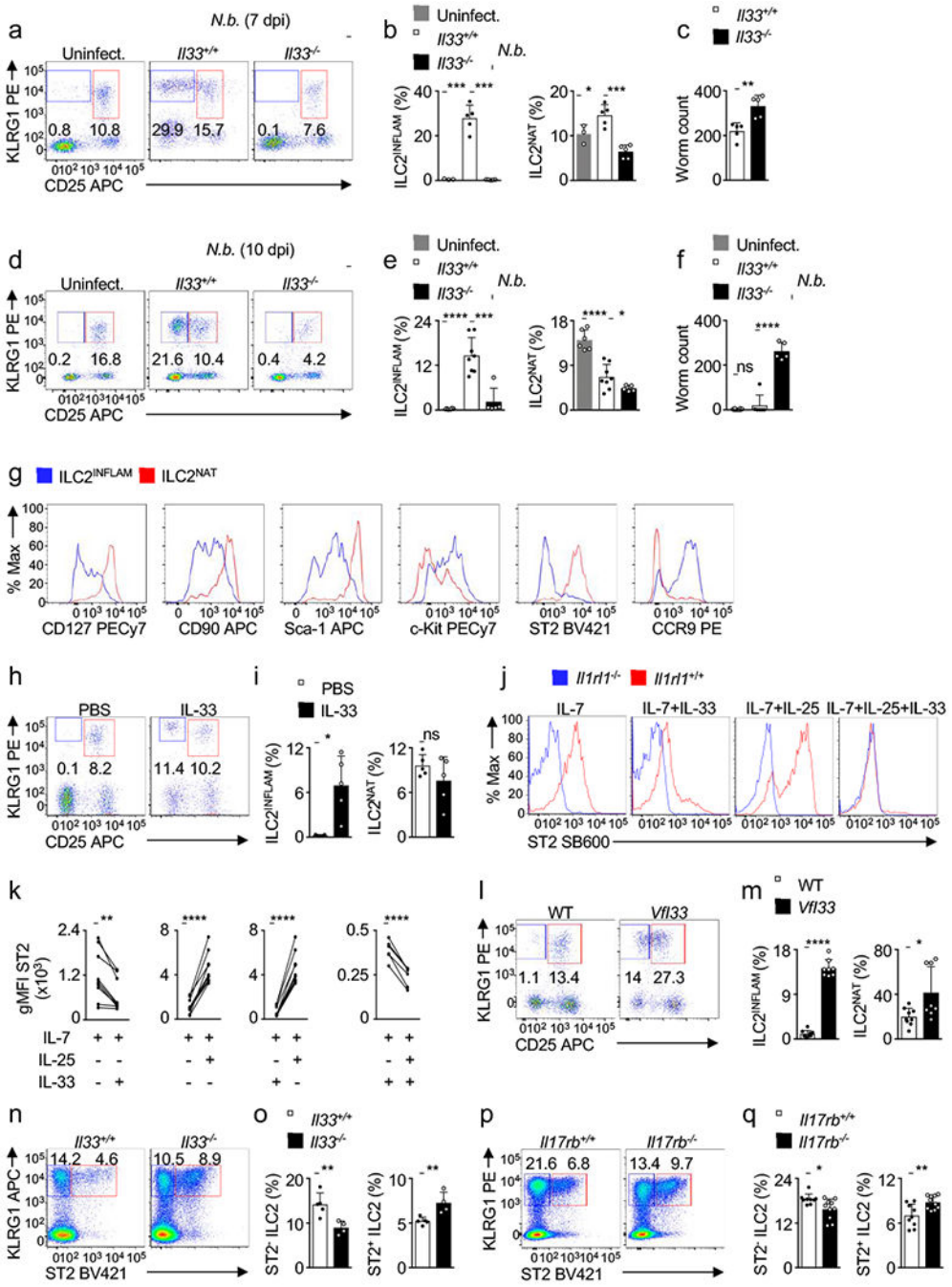

Figure 1: IL-33 regulates inflammatory ILC2s

(a-c) *Il33*$^{+/+}$ and *Il33*$^{-/-}$ mice were infected with *N. brasiliensis* or left uninfected and analyzed on day 7. (a) Flow cytometry plots of ILC2s from mesenteric lymph nodes. Cells are gated on Lin^{-} CD45^{+} lymphocytes. Numbers denote percentage of cells in each gate. dpi: day post-infection. (b) Percentage (Mean + SD, uninfected n=3, *Il33*$^{+/+}$ n=5 and *Il33*$^{-/-}$ n=5) of KLRG1^{+} CD25^{-} (ILC2^{INFLAM}) and KLRG1^{+} CD25^{+} ILC2s (ILC2^{NAT}) among Lin^{-} cells in the mesenteric lymph nodes. (c) Worm burden in the small intestine. Each symbol represents data from one mouse. Data are pooled from two independent experiments. (d-f)

Il33$^{+/+}$ and *Il33*$^{-/-}$ mice were infected with *N. brasiliensis* or left uninfected and analyzed on day 10. (d) Flow cytometry plots of ILC2s from mesenteric lymph nodes. Cells are gated on Lin$^-$ CD45$^+$ lymphocytes. Numbers denote percentage of cells in each gate. dpi: day post-infection. (e) Percentage (Mean + SD, uninfected n=6, *Il33*$^{+/+}$ n=8 and *Il33*$^{-/-}$ n=5) of KLRG1$^+$ CD25$^-$ (ILC2^{INFLAM}) and KLRG1$^+$ CD25$^+$ ILC2s (ILC2^{NAT}) among Lin$^-$ cells in the mesenteric lymph nodes. (f) Worm burden in the small intestine. Each symbol represents data from one mouse. Data are representative of two independent experiments.

(g) Wild-type mice were infected with *N. brasiliensis* and analyzed on day 7. Flow cytometry histogram overlays of surface marker expression in inflammatory (ILC2^{INFLAM}, blue) and natural (ILC2^{NAT}, red) ILC2s. Cells are gated on Lin$^-$ CD45$^+$ lymphocytes, KLRG1$^+$ CD25$^-$ (ILC2^{INFLAM}) and KLRG1$^+$ CD25$^+$ (ILC2^{NAT}). Data are representative of two independent experiments.

(h,i) Wild-type mice were injected with PBS or IL-33 for three consecutive days and analyzed one day later. (h) Flow cytometry plots of ILC2s from mesenteric lymph nodes. Cells are gated on Lin$^-$ CD45$^+$ lymphocytes. Numbers denote percentage of cells in each gate. (i) Percentage (Mean + SD, n=5) of KLRG1$^+$ CD25$^-$ (ILC2^{INFLAM}) and KLRG1$^+$ CD25$^+$ (ILC2^{NAT}) cells among Lin$^-$ cells in the mesenteric lymph nodes. Each symbol represents data from one mouse. Data are representative of three independent experiments.

(j,k) Small intestinal ILC2s from *Il1rl1*$^{+/+}$ and *Il1rl1*$^{-/-}$ mice were sorted and cultured *in vitro* for 3 days in the presence of the indicated combination of cytokines. (j) Flow cytometry histogram overlays of surface ST2 expression. Cells are gated on live lymphocytes. (k) ST2 geometric mean fluorescence intensity (gMFI) on ILC2s from *Il1rl1*$^{+/+}$ mice (n=9 for all except IL-25 and IL-33 n=6). Each symbol represents paired data from one mouse. Data are pooled from three independent experiments.

(l,m) ILC2s from mesenteric lymph nodes of *Vfl33* transgenic and wild-type (WT) mice. (l) Flow cytometry plots of ILC2s from mesenteric lymph nodes of *Vfl33* transgenic and WT mice. Cells are gated on Lin$^-$ CD45$^+$ lymphocytes. Numbers denote percentage of cells in each gate. (m) Percentage (Mean + SD, WT n=9 and *Vfl33* n=8) of KLRG1$^+$ CD25$^-$ (ILC2^{INFLAM}) and KLRG1$^+$ CD25$^+$ (ILC2^{NAT}) cells among Lin$^-$ cells in the mesenteric lymph nodes. Each symbol represents data from one mouse. Data are from two independent experiments combined.

(n,o) ILC2s from small intestinal lamina propria of *Il33*$^{+/+}$ and *Il33*$^{-/-}$ mice. (n) Flow cytometry plots of ILC2s from small intestinal lamina propria of *Il33*$^{+/+}$ and *Il33*$^{-/-}$ mice. Cells are gated on Lin$^-$ CD45$^+$ lymphocytes. Numbers denote percentage of cells in each gate. (o) Percentage (Mean + SD, *Il33*$^{+/+}$ n=5 and *Il33*$^{-/-}$ n=4) of KLRG1$^+$ ST2$^-$ and KLRG1$^+$ ST2$^+$ cells among Lin$^-$ cells in the small intestinal lamina propria. Each symbol represents data from one mouse. Data are from two independent experiments.

(p,q) ILC2s from small intestinal lamina propria of *Il17rb*$^{+/+}$ and *Il17rb7*$^{-/-}$ mice. (p) Flow cytometry plots of ILC2s from small intestinal lamina propria of *Il17rb*$^{+/+}$ and *Il17rb*$^{-/-}$ mice. Cells are gated on Lin$^-$ CD45$^+$ lymphocytes. Numbers denote percentage of cells in each gate. (q) Percentage (Mean + SD, *Il17rb*$^{+/+}$ n=9 and *Il17rb*$^{-/-}$ n=10) of KLRG1$^+$ ST2$^-$ and KLRG1$^+$ ST2$^+$ cells among Lin$^-$ cells in the small intestinal lamina propria. Each symbol represents data from one mouse. Data are from two independent experiments combined. *p < 0.05, **p < 0.01, ***p < 0.001, ****p < 0.0001 and n.s., not significant. See also Suppl. Fig. 1.

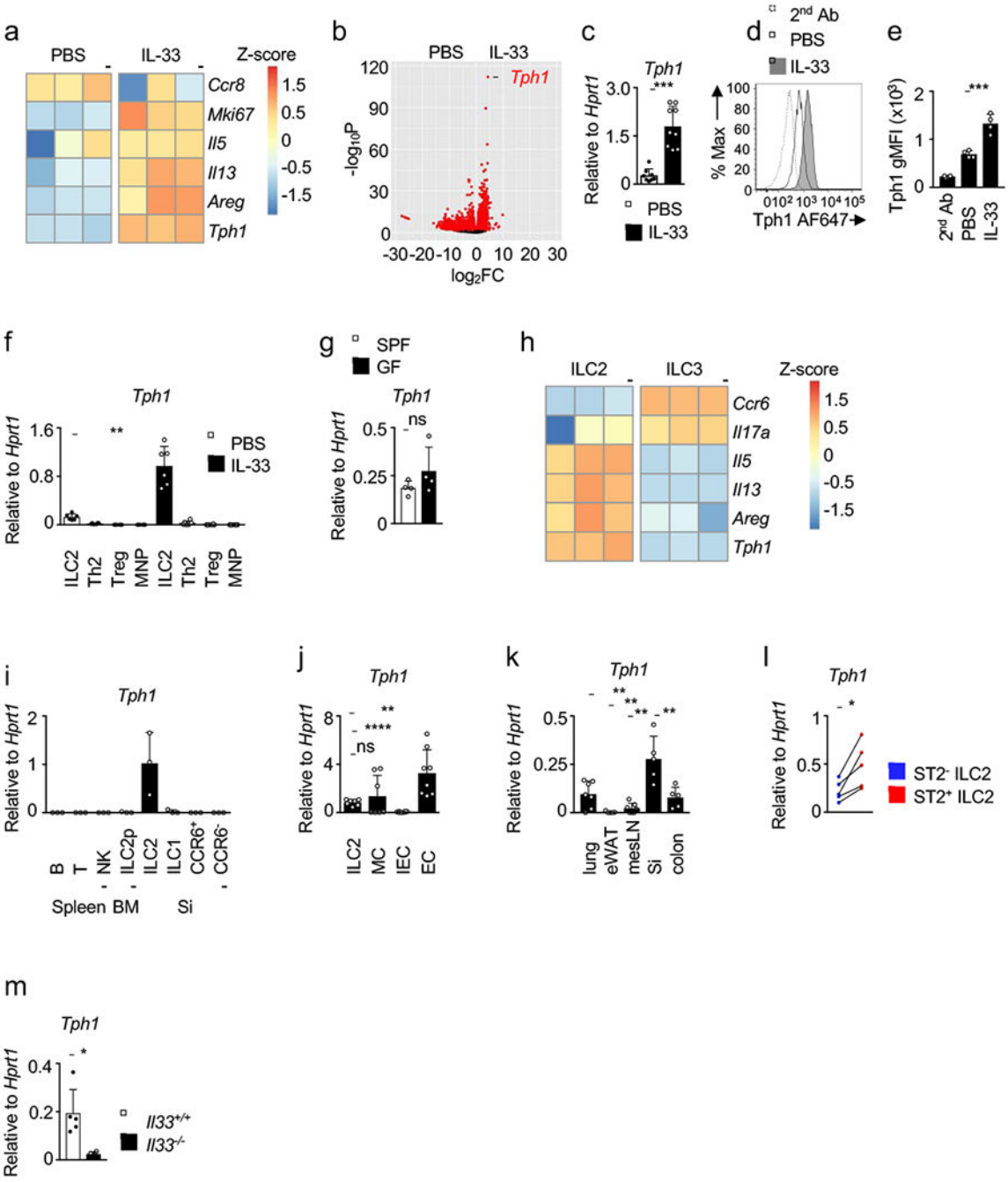

Figure 2: Tph1 is expressed in ILC2s and up-regulated upon cell activation

(a) Heat map of the indicated gene expression Z-scores of small intestinal ILC2s from PBS- or IL-33-treated wild-type mice as measured by RNA-seq. Each column represents a single mouse.

(b) RNA-seq volcano plot of differential gene expression between small intestinal ILC2s from IL-33- (positive log2FC) and PBS- (negative log^{2}FC) treated wild-type mice. FC: fold change.

(c) Expression of *Tph1* in ILC2s sorted from small intestine of PBS- or IL-33-treated wild-type mice as determined by qPCR analysis (Mean + SD, PBS n= 8 and IL-33 n= 9). Each symbol represents data from one mouse. Data are from three independent experiments combined.

(d,e) Tph1 expression in small intestinal ILC2s. (d) Flow cytometry histogram overlays of Tph1 expression in small intestinal ILC2s. Cells are gated on Lin^- $CD45^+$ $KLRG1^+$ lymphocytes. (e) Tph1 mean fluorescence intensity (MFI) (Mean + SD, n= 4). Each symbol represents data from one mouse. Data are representative of two independent experiments.

(f) Expression of *Tph1* in various cell subsets sorted from small intestine of PBS- or IL-33-treated $Il4^{Gfp/Gfp}$ mice as determined by qPCR analysis (Mean + SD, n= 6). MNP: mononuclear phagocytes; Each symbol represents data from one mouse. Data are from two independent experiments combined.

(g) Expression of *Tph1* in small intestinal ILC2s from germ-free (GF) mice and mice kept under specific-pathogen-free (SPF) conditions as determined by qPCR analysis (Mean + SD, n= 4). Each symbol represents data from one mouse.

(h) Heat map of the indicated gene expression Z-scores of small intestinal ILC2s and ILC3s from wild-type mice as measured by RNA-seq. Each column represents a single mouse.

(i) Expression of *Tph1* in the indicated sorted lymphocyte populations from wild-type mice as determined by qPCR analysis (Mean + SD, n= 3). Spleen B, T cells and NK: natural killer cells; bone marrow ILC2p: ILC2 progenitors; small intestinal ILC1s, ILC2s, $CCR6^+$ and $CCR6^-$ ILC3s. Each symbol represents data from one mouse. Data are representative of three biological replicates.

(j) Expression of *Tph1* in various cell subsets sorted from small intestine of wild-type mice as determined by qPCR analysis (Mean + SD, n= 7-8). MC: mast cells; IEC: intestinal epithelial cells; EC: enterochromaffin cells. Each symbol represents data from one mouse. Data are from two independent experiments combined.

(k) Expression of *Tph1* in sorted ILC2s from the indicated organs of wild-type mice as determined by qPCR analysis (Mean + SD, n= 5-7). eWAT: epididymal white adipose tissue; mesLN: mesenteric lymph nodes; Si: small intestine. Each symbol represents data from one mouse. Data are from three independent experiments combined.

(l) Expression of *Tph1* in sorted $KLRG1^+$ $ST2^-$ ILC2s and $KLRG1^+$ $ST2^+$ ILC2s from small intestine of wild-type mice as determined by qPCR analysis (Mean + SD, n= 5). Each symbol pair represents data from one mouse. Data are representative of two independent experiments.

(m) Expression of *Tph1* in sorted small intestinal ILC2s from $Il33^{+/+}$ and $Il33^{-/-}$ mice as determined by qPCR analysis (Mean + SD, $Il33^{+/+}$ n= 5 and $Il33^{-/-}$ n= 4). Each symbol represents data from one mouse. Data are representative of two independent experiment combined. *p < 0.05, **p < 0.01, ***p < 0.001, ****p < 0.0001 and n.s., not significant. See also Suppl. Fig. 2.

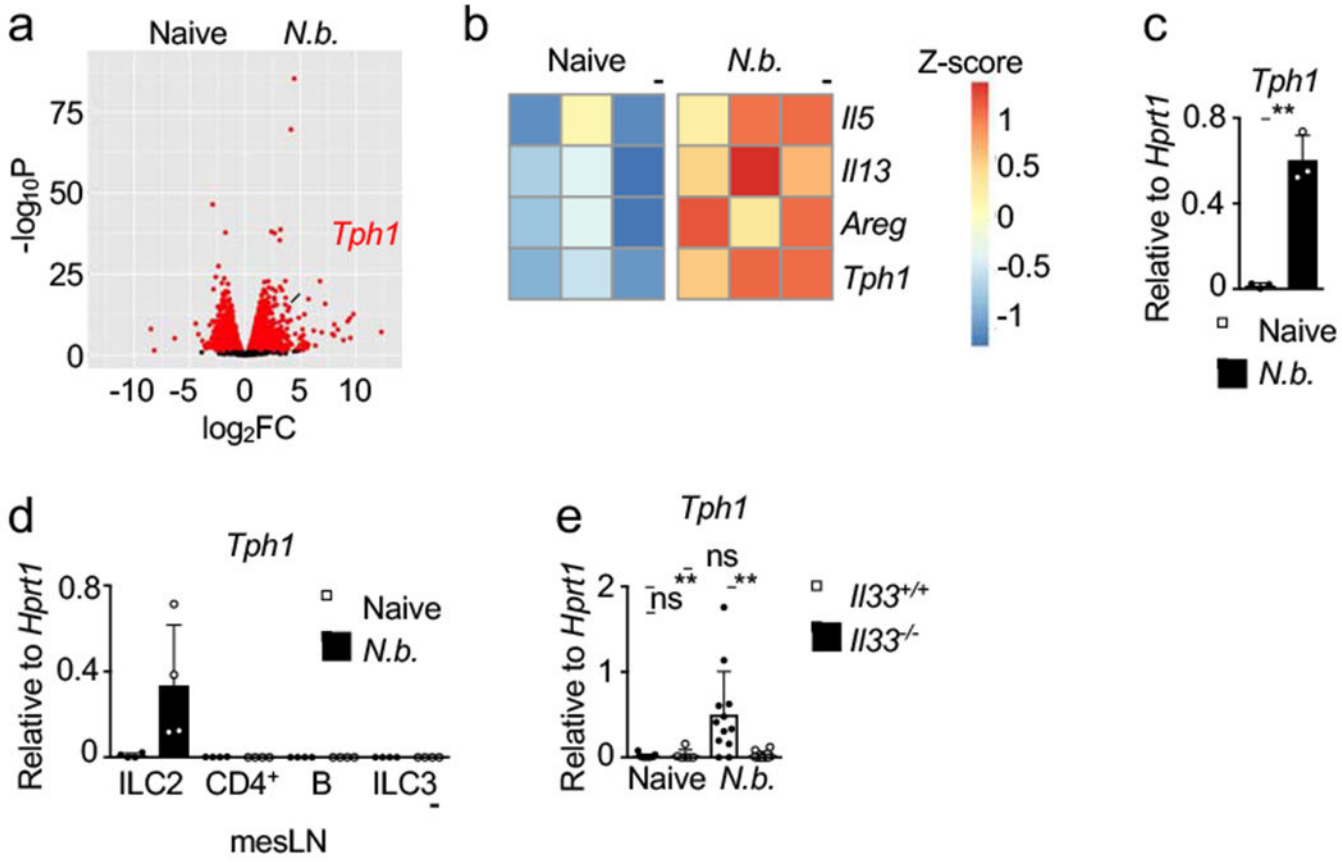

Figure 3: Helminth infection induces *Tph1* up-regulation in ILC2s, which is dependent on IL-33

(a) RNA-seq volcano plot of differential gene expression between ILC2s from mesenteric lymph nodes of naïve (negative log_2FC) and *N. brasiliensis* (*n.b.*)-infected (positive log_2FC) wild-type mice. FC: fold change.

(b) Heat map of the indicated gene expression Z-scores of ILC2s from mesenteric lymph nodes of naïve and *N. brasiliensis* (*N.b.*)-infected wild-type mice as measured by RNA-seq. Each column represents a single mouse.

(c) Expression of *Tph1* in sorted ILC2s from mesenteric lymph nodes of naïve and *N. brasiliensis* (*N.b.*)-infected wild-type mice as determined by qPCR analysis (Mean + SD, n= 3). Each symbol represents data from one mouse. Data are representative of three independent experiments.

(d) Expression of *Tph1* in sorted ILC2s and the indicated lymphocyte populations from mesenteric lymph nodes (mesLN) of naïve and *N. brasiliensis-infected* wild-type mice as determined by qPCR analysis (Mean + SD, n= 4). mesLN: mesenteric lymph nodes. Each symbol represents data from one mouse. Data are representative of four biological replicates.

(e) Expression of *Tph1* in sorted ILC2s from mesenteric lymph nodes of naïve and *N. brasiliensis* (*N.b.*)-infected *Il33*$^{+/+}$ and *Il33*$^{-/-}$ mice as determined by qPCR analysis. (Mean + SD, n= 5-12). Each symbol represents data from one mouse. Data are from three independent experiments combined. **p < 0.01, and n.s., not significant.

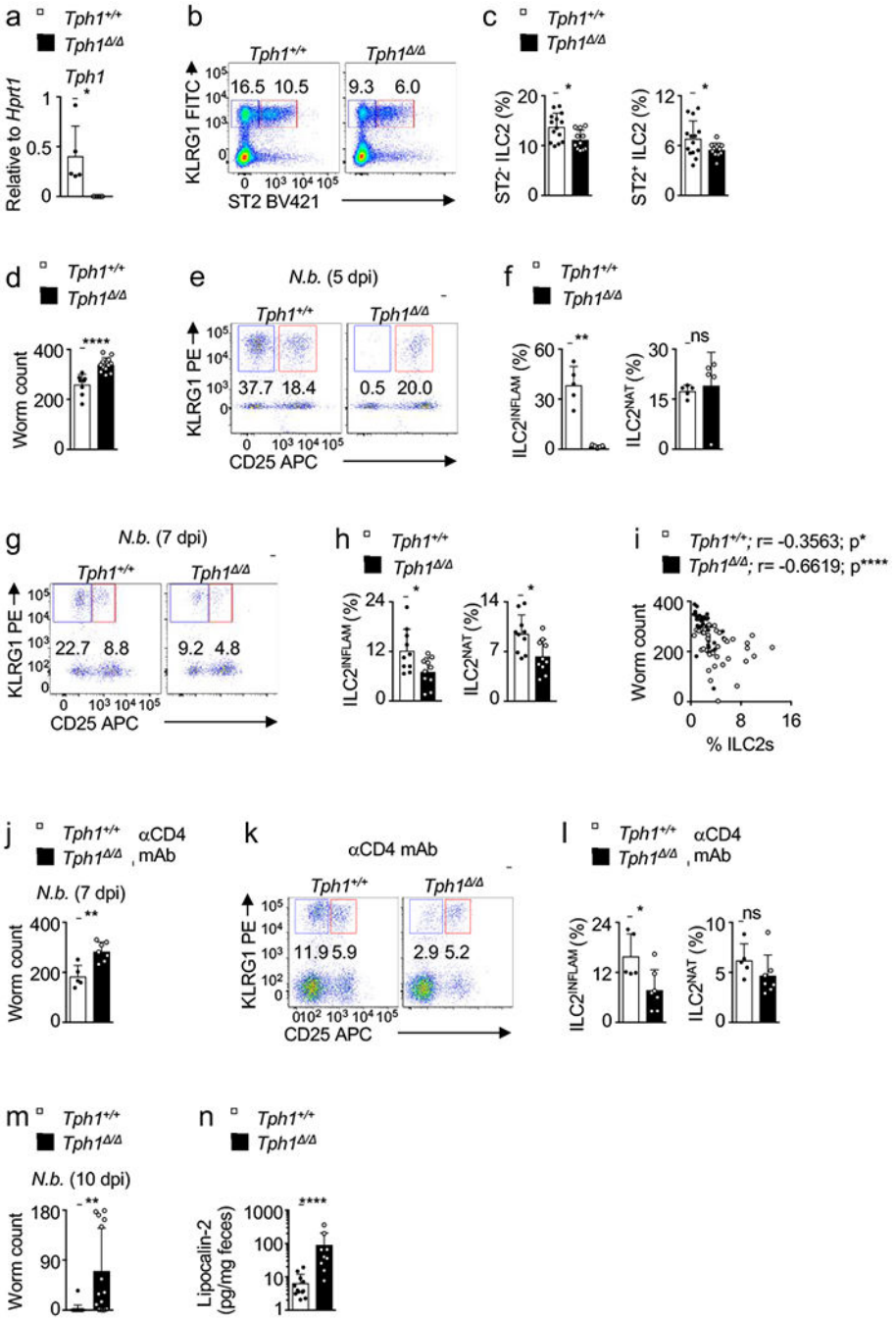

Figure 4: Mice with specific deletion of *Tph1* in lymphocytes are susceptible to *N. brasiliensis* infection and have reduced inflammatory ILC2 response

(a) Expression of *Tph1* (Mean + SD, n= 4) in sorted ILC2s from small intestine of $Tph1^{+/+}$ and $Tph1^{\Delta/\Delta}$ mice as determined by qPCR analysis. Each symbol represents data from one mouse. Data are representative of two independent experiments.

(b,c) ILC2s from small intestinal lamina propria of $Tph1^{+/+}$ and $Tph1^{\Delta/\Delta}$ mice. (b) Flow cytometry plots of ILC2s from small intestinal lamina propria of $Tph1^{+/+}$ and $Tph1^{\Delta/\Delta}$ mice. Cells are gated on Lin^{-} $CD45^{+}$ lymphocytes. Numbers denote percentage of cells in each gate. (c) Percentage (Mean + SD, $Tph1^{+/+}$ n=14 and $Tph1^{\Delta/\Delta}$ n=11) of $KLRG1^{+}$ $ST2^{-}$ ILC2s

and KLRG1^{+} ST2^{+} ILC2s cells among Lin^{-} cells in the small intestinal lamina propria. Each symbol represents data from one mouse. Data are from three independent experiments combined.

(d) *Tph1*$^{+/+}$ and *Tph1*$^{\Delta/\Delta}$ mice were infected with *N. brasiliensis* and analyzed on day 7. Worm burden in the small intestine (Mean + SD, *Tph1*$^{+/+}$ n= 8, *Tph1*$^{+/+}$ n= 12). Each symbol represents data from one mouse. Data are representative of four independent experiments.

(e,f) *Tph1*$^{+/+}$ and *Tph1*$^{\Delta/\Delta}$ mice were infected with *N. brasiliensis* and analyzed on day 5. (e) Flow cytometry plots of ILC2s from mesenteric lymph nodes. Cells are gated on Lin^{-} CD45^{+} lymphocytes. Numbers denote percentage of cells in each gate. dpi: day post-infection. (f) Percentage (Mean + SD, n= 5) of KLRG1^{+} CD25^{-} (ILC2^{INFLAM}) and KLRG1^{+} CD25^{+} (ILC2^{NAT}) cells among Lin^{-} cells in the mesenteric lymph nodes. Each symbol represents data from one mouse. Data are representative of three independent experiments.

(g,h) *Tph1*$^{+/+}$ and *Tph1*$^{\Delta/\Delta}$ mice were infected with *N. brasiliensis* and analyzed on day 7. (g) Flow cytometry plots of ILC2s from mesenteric lymph nodes. Cells are gated on Lin^{-} CD45^{+} lymphocytes. Numbers denote percentage of cells in each gate. dpi: day post-infection. (h) Percentage (Mean + SD, n= 10) of KLRG1^{+} CD25^{-} (ILC2^{INFLAM}) and KLRG1^{+} CD25^{+} (ILC2^{NAT}) cells among Lin^{-} cells in the mesenteric lymph nodes. Each symbol represents data from one mouse. Data are from two independent experiments combined.

(i) Correlation between percentage of ILC2s and worm burden (Mean + SD, *Tph1*$^{+/+}$ n= 35 and *Tph1*$^{\Delta/\Delta}$ n= 37). Spearman correlation coefficient r are indicated. Each symbol represents data from one mouse. Data are from four independent experiments combined.

(j-l) *Tph1*$^{+/+}$ and *Tph1*$^{\Delta/\Delta}$ mice were infected with *N. brasiliensis* and treated with an anti-CD4 depleting antibody and analyzed on day 7. (j) Worm burden in the small intestine. dpi: day post-infection. (k) Flow cytometry plots of ILC2s from mesenteric lymph nodes. Cells are gated on Lin^{-} CD45^{+} lymphocytes. Numbers denote percentage of cells in each gate. (l) Percentage (Mean + SD, *Tph1*$^{+/+}$ n=5 and *Tph1*$^{\Delta/\Delta}$ n=7) of KLRG1^{+} CD25^{-} (ILC2^{INFLAM}) cells KLRG1^{+} CD25^{+} (ILC2^{NAT}) among Lin^{-} cells in the mesenteric lymph nodes. Each symbol represents data from one mouse. Data are representative of two independent experiments.

(m,n) *Tph1*$^{+/+}$ and *Tph1*$^{\Delta/\Delta}$ mice were infected with *N. brasiliensis* and analyzed on day 10. (m) Worm burden in the small intestine (Mean + SD, *Tph1*$^{+/+}$ n= 22, *Tph1*$^{\Delta/\Delta}$ n= 14). Each symbol represents data from one mouse. Data are from three independent experiments combined dpi: day post-infection. (n) Lipocalin in feces measured by ELISA (Mean + SD, *Tph1*$^{+/+}$ n= 12, *Tph1*$^{\Delta/\Delta}$ n= 9). Each symbol represents data from one mouse. Data are from two independent experiments combined. *p < 0.05, **p < 0.01, ****p < 0.0001 and n.s., not significant. See also Suppl. Fig. 3.

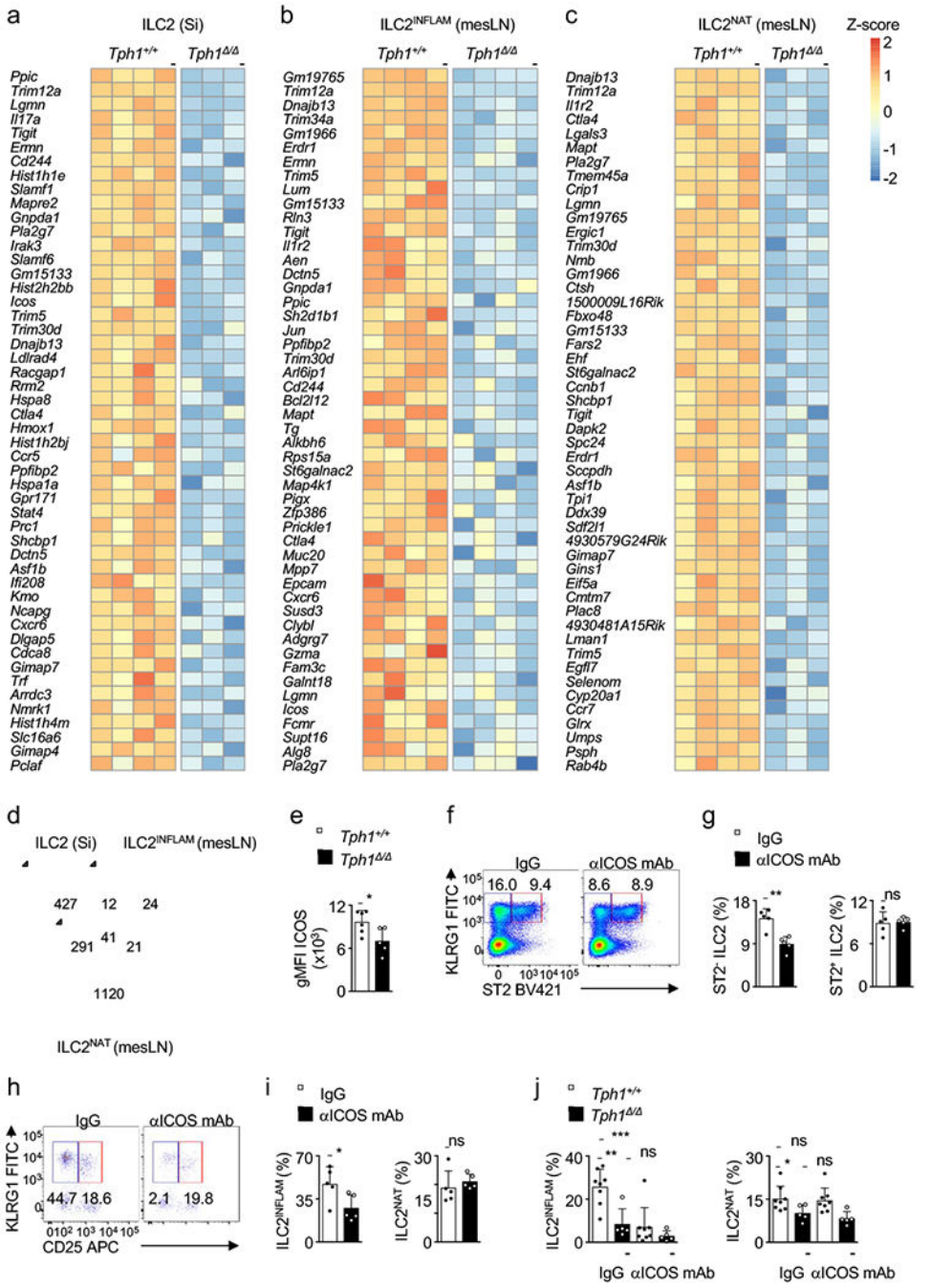

Figure 5: *Tph1*$^{\Delta/\Delta}$ mice have defective ILC2 activation

(a-d) RNA-seq of sorted ILC2s from the small intestine and ILC2^{INFLAM} and ILC2^{NAT} from mesenteric lymph nodes of *Tph1*$^{+/+}$ and *Tph1*$^{\Delta/\Delta}$ mice on day 7 after *N. brasiliensis* infection. (a-c) Heat maps showing expression of the 50 genes most significantly down-regulated (smallest p value) in *Tph1*$^{\Delta/\Delta}$ as measured by RNA-seq. Heat map color indicates row Z score of $\log_{10}$(normalized counts + 1). Each column represents a single mouse. Si: small intestine; mesLN: mesenteric lymph nodes. (a) (Si: *Tph1*$^{+/+}$ n= 4 and *Tph1*$^{\Delta/\Delta}$ n= 3). (b) (mesLN ILC2^{INFLAM}: *Tph1*$^{+/+}$ n= 4 and *Tph1*$^{\Delta/\Delta}$ n= 4). (c) mesLN ILC2^{NAT}: *Tph1*$^{+/+}$

n= 4 and *Tph1*$^{\Delta/\Delta}$ n= 3). (d) Venn diagram of the significantly differentially expressed genes down-regulated in *Tph1*$^{\Delta/\Delta}$ mice for each ILC2 population. Numbers denote the numbers of differentially expressed genes. Si: small intestine; mesLN: mesenteric lymph nodes.
(e) ICOS geometric mean fluorescent intensity (gMFI) on KLRG1^{+} CD25^{-} ILC2s from the mesenteric lymph nodes of *Tph1*$^{+/+}$ and *Tph1*$^{\Delta/\Delta}$ mice on day 7 after *N. brasiliensis* infection (*Tph1*$^{+/+}$ n= 6 and *Tph1*$^{\Delta/\Delta}$ n= 5). Each symbol represents data from one mouse. Data are representative of two independent experiments.
(f,g) Wild-type mice were treated with an anti-ICOS blocking antibody or isotype control (IgG) and analyzed on day 7. (f) Flow cytometry plots of ILC2s from intestinal lamina propria. Cells are gated on Lin^{-} CD45^{+} lymphocytes. Numbers denote percentage of cells in each gate. (g) Percentage (Mean + SD, n= 5) of KLRG1^{+} ST2^{-} ILC2s and KLRG1^{+} ST2^{+} ILC2s among Lin^{-} cells in intestinal lamina propria. Cells are gated on Lin^{-} CD45^{+} lymphocytes. Each symbol represents data from one mouse. Data are representative of three independent experiments.
(h,i) Wild-type mice were infected with *N. brasiliensis* and treated with an anti-ICOS blocking antibody or isotype control (IgG) and analyzed on day 5. (h) Flow cytometry plots of ILC2s from mesenteric lymph nodes. Cells are gated on Lin^{-} CD45^{+} lymphocytes. Numbers denote percentage of cells in each gate. (i) Percentage (Mean + SD, n= 5) of KLRG1^{+} CD25^{-} (ILC2^{INFLAM}) and KLRG1^{+} CD25^{+} (ILC2^{NAT}) cells among Lin^{-} cells in the mesenteric lymph nodes. Cells are gated on Lin^{-} CD45^{+} lymphocytes. Each symbol represents data from one mouse. Data are representative of two independent experiments.
(j) *Tph1*$^{+/+}$ and *Tph1*$^{\Delta/\Delta}$ mice were infected with *N. brasiliensis* and treated with an anti-ICOS blocking antibody or isotype control (IgG) and analyzed on day 5. Percentage (Mean + SD, *Tph1*$^{+/+}$ + IgG n=8 *Tph1*$^{\Delta/\Delta}$ + IgG n= 5, *Tph1*$^{+/+}$ + anti-ICOS n=8 and *Tph1*$^{\Delta/\Delta}$ anti-ICOS n= 5) of KLRG1^{+} CD25^{-} (ILC2^{INFLAM}) and KLRG1^{+} CD25^{+} (ILC2^{NAT}) cells among Lin^{-} cells in the mesenteric lymph nodes. Cells are gated on Lin^{-} CD45^{+} lymphocytes. Each symbol represents data from one mouse. Data are representative of four independent experiments. *p < 0.05, **p < 0.01, ***p < 0.001 and n.s., not significant. See also Suppl. Fig. 4.

KEY RESOURCES TABLE

REAGENT or RESOURCE	SOURCE	IDENTIFIER
Antibodies		
Anti-mouse CD16/32 (93)-Purified	Biolegend	Cat#101302
Anti-mouse CD3e (145-2C11)-PerCP-Cy5.5	eBioscience	Cat#45-0031-82
Anti-mouse CD3e (145-2C11)-PE-Cyanine7	eBioscience	Cat#25-0031-82
Anti-mouse CD5 (53-7.3)-PerCP-Cy5.5	eBioscience	Cat#45-0031-82
Anti-mouse CD5 (53-7.3)-PE-Cyanine7	eBioscience	Cat#25-0051-81
Anti-mouse FcεRI (Mar-1)-PerCP-Cy5.5	eBioscience	Cat#46-5898-82
Anti-mouse FcεRI (Mar-1)-APC	eBioscience	Cat#17-5898-82
Anti-mouse NK1.1 (PK136)-Alexa Fluor 700	eBioscience	Cat#56-5941-82
Anti-mouse NKp46 (29A1.4)-Alexa Fluor 700	eBioscience	Cat#56-3351-82
Anti-mouse B220 (RA3-6B2)-APC-eFluor 780	eBioscience	Cat#47-0452-82
Anti-mouse CD19 (eBio1D3 (1D3))-PerCP-Cy5.5	eBioscience	Cat#45-0193-82
Anti-mouse CD11b (M1/70)-APC-eFluor 780	eBioscience	Cat#47-0112-82
Anti-mouse CD11b (M1/70)-Alexa Fluor 700	eBioscience	Cat#56-0112-82
Anti-mouse CD11c (N418)-APC-eFluor 780	eBioscience	Cat#47-0114-82
Anti-mouse KLRG1 (2F1)-PE	eBioscience	Cat#12-5893-82
Anti-mouse KLRG1 (2F1)-FITC	eBioscience	Cat#11-5893-82
Anti-mouse KLRG1 (2F1)-APC	eBioscience	Cat#17-5893-82
Anti-mouse KLRG1 (2F1)-BV605	eBioscience	Cat#138419
Anti-mouse CD45 (30-F11)-BUV395	BD Biosciences	Cat#564279
Anti-mouse CD45 (30-F11)-BV605	Biolegend	Cat#103140
Anti-mouse CD4 (GK1.5)-BV421	Biolegend	Cat#100438
Anti-mouse CD4 (RM4-5)-BV421	Biolegend	Cat#100543
Anti-mouse CD4 (RM4-5)-BV650	Biolegend	Cat#100546
Anti-mouse CD4 (RM4-5)-BV605	Biolegend	Cat#100547
Anti-mouse CD8α (53-6.7)-BV650	Biolegend	Cat#100742
Anti-mouse CD8α (53-6.7)-BV605	Biolegend	Cat#100743
Anti-mouse Sca-1 (D7)-APC	eBioscience	Cat#17-5981-82
Anti-mouse c-Kit (2B8)-PE-Cyanine7	eBioscience	Cat#25-1171-82
Anti-mouse CD25 (PC61.5)-APC	eBioscience	Cat#17-0251-82
Anti-mouse CD25 (PC61.5)- PE-Cyanine7	eBioscience	Cat#25-0251-82
Anti-mouse CD127 (A7R34)-PE-Cyanine7	eBioscience	Cat#25-1271-82
Anti-mouse CD127 (A7R34)-BV421	Biolegend	Cat#135024
Anti-mouse CCR9 (9B1)-FITC	Biolegend	Cat#129706
Anti-mouse CCR9 (9B1)-PE	Biolegend	Cat#129708
Anti-mouse CD90.2 (53-2.1)-FITC	Biolegend	Cat#140304
Anti-mouse CD90.2 (HIS51)-APC	eBioscience	Cat#17-0900-82

REAGENT or RESOURCE	SOURCE	IDENTIFIER
Anti-mouse ICOS (7E.17G9)-PE	eBioscience	Cat#12-9942-82
Anti-mouse ST2 (RMST2-2)-Biotinylated	eBioscience	Cat#13-9333-82
Anti-mouse ST2 (RMST2-2)-SB600	eBioscience	Cat#63-9335-82
Anti-mouse CD326 (G8.8)-FITC	eBioscience	Cat#11-5791-82
Anti-mouse CD326 (G8.8)-APC	eBioscience	Cat#17-5791-82
Anti-mouse CD24 (M1/69)-PE	eBioscience	Cat#12-0242-82
Anti-mouse CD24 (M1/69)-BV421	Biolegend	Cat#101825
Anti-mouse MHC Class II (I-A/I-E) (M5/115.15.2)-eF450	eBioscience	Cat#48-5321-82
Anti-mouse GATA3 (TWAJ)	eBioscience	Cat#46-9966-42
Anti-mouse Tph1 (EP1311Y)	OriGene	Cat#TA300818
Anti-mouse ICOS antibody-Purified	Bioxcell	Cat#BE0059
Rat IgG isotype control-Purified	Sigma-Aldrich	Cat#I4131
Anti-mouse CD4 antibody (GK1.5)-Purified	This paper	N/A
Streptavidin-BV421	Biolegend	Cat#405225
Streptavidin-BV605	Biolegend	Cat#405229
Streptavidin-BV650	Biolegend	Cat#405232
Streptavidin-Alexa Fluor 647	Thermo Fisher Scientific	Cat#S32357
Mouse anti-serotonin (H209)	Dako	Cat#M0758
Hamster anti-CD3ε (eBio500A2)-biotinylated	eBioscience	Cat#13-0033-82
Polyclonal goat anti-mouse IL-33	R&D Systems	Cat#AF3626
Mouse anti-E-Cadherin (36/E-Cadherin)-Alexa Fluor 647	BD Pharmingen	Cat#560062
Donkey anti-goat IgG-Alexa 488	Thermo Fisher Scientific	Cat#A-11055
Goat anti-mouse IgG1-Alexa 488	Thermo Fisher Scientific	Cat#A-21121
DAPI	Thermo Fisher Scientific	Cat#D1306
Hepes (1 M)	Gibco	Cat#15630080
Sodium pyruvate (100 mM)	Gibco	Cat#11360070
MEM non-essential amino acid solution (100X)	Gibco	Cat#11140050
L-Glutamine (200 mM)	Gibco	Cat#25030081
Penicillin- Streptomycin (10,000 U/mL)	Gibco	Cat#15140122
Dulbecco's Modified Eagle Medium	Gibco	Cat#41965039
RPMI 1640 with L-glutamine	Corning	Cat#10-040-CV
Percoll	GE Healthcare	Cat#GE17-0891-01
BSA	Sigma-Aldrich	Cat#A6003
ACK lysing buffer	Lonza	Cat#12002-070
EDTA	Thermo Fisher Scientific	Cat#15575020
Bacterial and Virus Strains		
Biological Samples		
Chemicals, Peptides, and Recombinant Proteins		
DTT	Sigma-Aldrich	Cat#43815; CAS: 3483-12-3

REAGENT or RESOURCE	SOURCE	IDENTIFIER
Dispase II	Thermo Fisher Scientific	Cat#17105041; CAS: 42613-33-2
Collagenase III	Worthington	Cat#LS004183; CAS 9001-12-1
Collagenase II	Sigma-Aldrich	Cat#C6885; CAS: 9001-12-1
DNaseI	Sigma-Aldrich	Cat#D5025; 9003-98-9
Liberase TM	Roche	Cat#5401127001; CAS: 9001-12-1
Trizol	Invitrogen	Cat#15596026
Recombinant mouse IL-2	R&D Systems	Cat#402-ML
Recombinant mouse IL-7	R&D Systems	Cat#407-ML
Recombinant mouse IL-33	R&D Systems	Cat#3626-ML/CF
Recombinant mouse IL-7	Biolegend	Cat#577802
Recombinant mouse IL-33	Biolegend	Cat#580502
Recombinant mouse IL-25	Biolegend	Cat#587302
Recombinant mouse IL-25	R&D Systems	Cat#1399-IL
10X Single-Cell Lysis Buffer	Clontech Laboratories	Cat#635013
Dextran-coated charcoal	Sigma-Aldrich	Cat#C6241
Tranylcypromine hemisulfate	Focus Biomolecules	Cat#10-4535; CAS: 13492-01-8
2-Mercaptoethanol	Gibco	Cat#21985023; CAS: 60-24-2
16% paraformaldehyde	Electron Microscopy Sciences	Cat#15710; CAS: 30525-89-4
Freezing medium OCT	Leica	Cat#14020108926
Triton X-100	Sigma-Aldrich	Cat#T8787; CAS: 9002-93-1
Protector RNase Inhibitor	Roche	Cat#3335402001
Critical Commercial Assays		
Live/Dead Fixable Aqua Dead Cell Stain Kit	Thermo Fisher Scientific	Cat#L34957
SYTOX Blue Dead Cell Stain	Thermo Fisher Scientific	Cat#S34857
Foxp3 transcription factor staining buffer set	eBioscience	Cat#00-5523-00
High Capacity cDNA Reverse Transcription kit	Applied Biosystems	Cat#4368814
TaqMan® Universal Master Mix II, with UNG	Applied Biosystems	Cat#4440038
Power SYBR™ Green PCR Master Mix	Applied Biosystems	Cat#4367660
SMARTer® Ultra® Low Input RNA Kit V4	Clontech Laboratories	Cat#634894
Lipocalin-2/NGAL DuoSet ELISA system	R&D Systems	Cat#DY1857
Ultra Sensitive Serotonin enzyme immunoassay	Labor Diagnostika Nord	Cat#BA E-5900
Deposited Data		
Small intestinal ILC2 and ILC3 RNA-seq data	This paper; Klose et al., 2017	GEO: GSE101625
Mesenteric lymph node ILC2 RNA-seq data	This paper; Moriyama et al., 2018	GEO: GSE108884
Raw and analyzed data	This paper	GEO: GSE145289
Experimental Models: Cell Lines		
Experimental Models: Organisms/Strains		
Mouse: B6: C57BL/6	The Jackson Laboratories	RRID:IMSR JAX:000664
Mouse: B6: *Tph1*$^{fl/fl}$	Yadav et al., 2008	N/A

REAGENT or RESOURCE	SOURCE	IDENTIFIER
Mouse: B6: *Ilr7*$^{Cre/+}$	Schlenner et al., 2010	N/A
Mouse: B6: *Il33*$^{-/-}$	Amgen Inc. through Taconic Farms; Louten et al., 2011	N/A
Mouse: B6: *Vfl33*	He et al., 2018	N/A
Mouse: B6: *Il17rb*$^{-/-}$	Neill et al., 2010	N/A
Mouse: B6: *Il1rl1*$^{-/-}$	Townsend et al., 2000	N/A
Mouse: BALB/c: *Il4*$^{Gfp/Gfp}$	Mohrs et al., 2001	N/A
Nippostrongylus brasiliensis	Lawrence et al., 1996	N/A
Oligonucleotides		
Tph1	Applied Biosystems	Cat#Mm01202614_m1
Chga	Applied Biosystems	Cat#Mm00514341_m1
Icos	Applied Biosystems	Cat#Mm00497600_m1
Cxcr6	Applied Biosystems	Cat#Mm00472858_m1
Tigit	Applied Biosystems	Cat#Mm03807522_m1
Htr1b	Applied Biosystems	Cat#Mm00439377_s1
Hprt1	Applied Biosystems	Cat#Mm00446968_m1
Trim12a (5′ CCTGTCTGTCTGAACCTGATGG 3′ and 5′ GGCTTGAACATTTTGAGCCTCT 3′)	Invitrogen	N/A
Ermn (5′ CTGAGACACTGAGCGGGAC 3′ and 5′ CAACCTTGTAGTATGCCTGGG 3′)	Invitrogen	N/A
Lgmn (5′ TGGACGATCCCGAGGATGG 3′ and 5′ GTGGATGATCTGGTAGGCGT3′)	Invitrogen	N/A
Il25	Qiagen	Cat#QT00134645
Il33	Qiagen	Cat#QT00135170
Actb	Qiagen	Cat#QT01136772
Recombinant DNA		
Software and Algorithms		
FACS Diva software	BD Biosciences	N/A
FlowJo V9.9.3 software	TreeStar	https://www.flowjo.com/solutions/flowjo/downloads
FlowJo V10.4.2 software	TreeStar	https://www.flowjo.com/solutions/flowjo/downloads
GraphPad Prism 7.0 software	GraphPad	https://www.graphpad.com
QuantStudio Real-Time PCR V1.0 software	Thermo Fisher Scientific	N/A
NanoDrop 2000 Spectrophotometer V1.0 software	Thermo Fisher Scientific	N/A
CASAVA (v2.17)	Illumina	N/A
FLEXBAR (v2.4)	Dodt et al., 2012	N/A
STAR aligner (v2.3.0)	Dobin et al., 2013	N/A
Rsubread R package	Liao et al., 2013	N/A
DESeq2 version 1.20.0	Love et al., 2014	N/A
clusterProfiler R package	Yu et al., 2012	N/A
Other		